

Changes in Atlantic Water Circulation Patterns and Volume Transports North of Svalbard Over the Last 12 Years (2008–2020)

Key Points:

- Twelve years of Mercator Ocean fields document the recent evolution in Atlantic Water (AW) pathways and properties in the Western Nansen Basin
- AW progressed further north following new pathways, over the Northern Yermak Plateau and further east above the 3,800 m isobath
- The boundary current became more unstable, with enhanced mesoscale activity, injecting AW basin-ward east of 18°E

Supporting Information:

- Supporting Information S1
- Movie S1

Correspondence to:

M. Athanase,
mathanase@locean-ipsl.upmc.fr

Citation:

Athanase, M., Provost, C., Artana, C., Pérez-Hernández, M. D., Sennéchaël, N., Bertosio, C., et al. (2021). Changes in Atlantic Water circulation patterns and volume transports North of Svalbard over the last 12 years (2008–2020). *Journal of Geophysical Research: Oceans*, 126, e2020JC016825. <https://doi.org/10.1029/2020JC016825>

Received 24 SEP 2020
Accepted 2 DEC 2020

Marylou Athanase¹ , Christine Provost¹ , Camila Artana² ,
M. Dolores Pérez-Hernández³ , Nathalie Sennéchaël¹ , Cécilia Bertosio¹ ,
Gilles Garric² , Jean-Michel Lellouche² , and Pierre Prandi⁴ 

¹Laboratoire LOCEAN-IPSL, Sorbonne Université (UPMC, Univ. Paris 6), CNRS, IRD, MNHN, Paris, France,

²MERCATOR-OCEAN, Parc Technologique du Canal, Ramonville Saint Agne, France, ³Unidad de Océano y Clima, Instituto de Oceanografía y Cambio Global, IOCAG, Universidad de Las Palmas de Gran Canaria, ULPGC-CSIC, Las Palmas de Gran Canaria, Spain, ⁴CLS, Parc Technologique du Canal, Ramonville Saint-Agne, France

Abstract Atlantic Water (AW) enters the Arctic through Fram Strait as the West Spitsbergen Current (WSC). When reaching the south of Yermak Plateau, the WSC splits into the Svalbard, Yermak Pass, and Yermak Branches. Downstream of Yermak Plateau, AW pathways remain unclear and uncertainties persist on how AW branches eventually merge and contribute to the boundary current along the continental slope. We took advantage of the good performance of the 1/12° Mercator Ocean model in the Western Nansen Basin (WNB) to examine the AW circulation and volume transports in the area. The model showed that the circulation changed in 2008–2020. The Yermak Branch (YB) strengthened over the northern Yermak Plateau, feeding the Return YB along the eastern flank of the Plateau. West of Yermak Plateau, the Transpolar Drift likely shifted westward while AW recirculations progressed further north. Downstream of the Yermak Plateau, an offshore current developed above the 3,800 m isobath, fed by waters from the Yermak Plateau tip. East of 18°E, enhanced mesoscale activity from the boundary current injected additional AW basin-ward, further contributing to the offshore circulation. A recurrent anticyclonic circulation developed in the Sofia Deep, which also occasionally fed the western part of the offshore flow. The intensification of the circulation coincided with an overall warming in the upper WNB (0–1,000 m), consistent with the progression of AW. This regional description of the changing circulation provides a background for the interpretation of upcoming observations.

Plain Language Summary Atlantic Water (AW) is the main source of heat and salt to the Arctic Ocean. We used 12 years of a high-resolution model to examine the recent evolution of the circulation, volume transport and properties of AW in their major entry region, the Western Nansen Basin (WNB). The model showed the development of new pathways of AW, the intensification of the circulation north of Svalbard, along with the progressive warming and thickening of the AW layer. These changes are important for the distribution of heat and salt to the Eurasian basin interior and for the sea-ice cover evolution.

1. Introduction

The Atlantic Water (AW), which flows along the west slope of Svalbard with the West Spitsbergen Current (WSC, red arrows on Figure 1) in Fram Strait, constitutes the largest source of heat and salt to the Arctic Ocean. The AW inflow varies seasonally, being stronger and warmer in winter than in summer (Beszczynska-Miller et al., 2012; V. V. Ivanov et al., 2009). A fraction of the AW carried by the WSC recirculates toward Fram Strait south of 81°N, mainly through eddies, and does not enter the Arctic Ocean (e.g., Hatterman et al., 2016). North of Svalbard, the WSC reaches the Yermak Plateau, and splits into three branches: the shallow Svalbard Branch (SB) circulating eastward, along the 400–500 m isobaths of the Svalbard continental slope (Cokelet et al., 2008; Muench et al., 1992; Sirevaag et al., 2011); the deeper Yermak Branch (YB), following the 1,500 m isobath along the western slope of Yermak Plateau (Manley, 1995; Manley et al., 1992); and the Yermak Pass Branch (YPB), flowing across the Yermak Plateau along the 700–800 m isobaths and constituting the major route for AW in winter (Figure 1; Crews et al., 2019; Koenig et al., 2017a; Menze

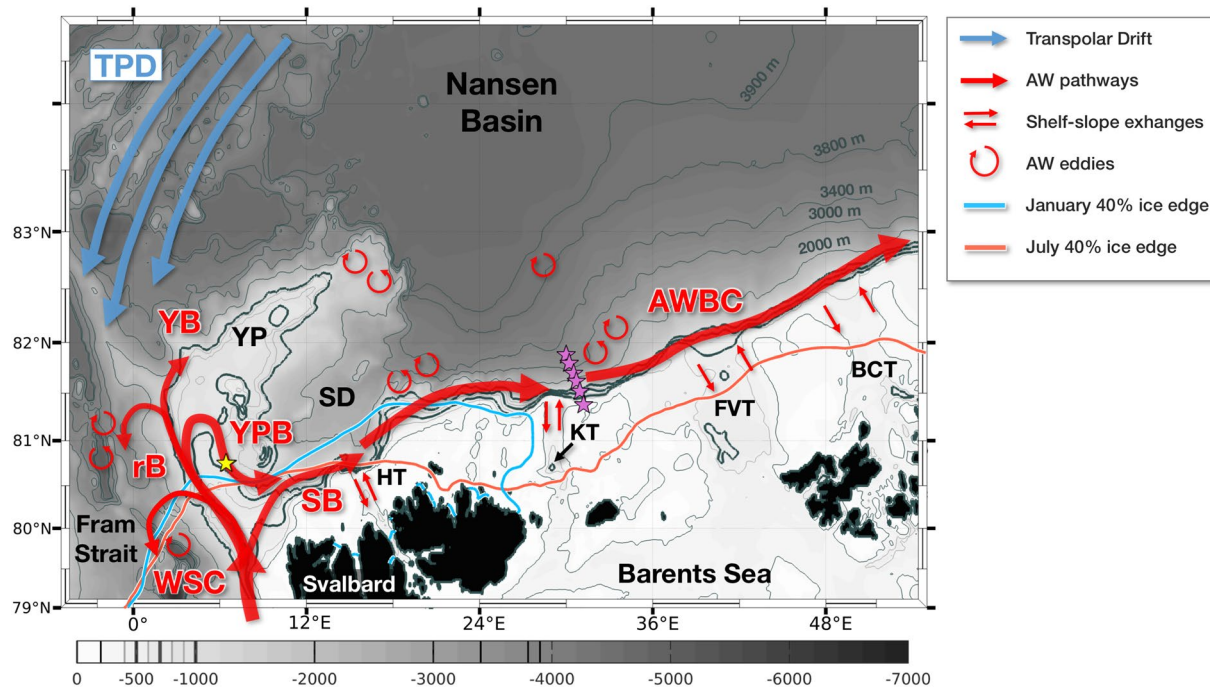


Figure 1. Schematic of the upper circulation in the Western Nansen Basin. IBCAO bathymetry is in greyscale. Red arrows correspond to the mean AW circulation in PSY4 over 2008–2010. Blue arrows represent the near-surface Transpolar Drift (TPD). Orange and blue contours are respectively the mean July and January ice edge (40% ice concentration) from PSY4 over 2008–2020. WSC, West Spitsbergen Current; SB, Svalbard Branch; YPB, Yermak Pass Branch; YB, Yermak Branch; AWBC, AW Boundary Current; rB, recirculation Branches; SD, Sofia Deep; YP, Yermak Plateau; HT, KT, FVT, and BCT, Hinlopen, Kvitoya, Franz-Victoria, and British Channel Troughs. Pink stars indicate the A-TWAIN moorings, the yellow star a recent mooring in the YPB.

et al., 2019). Water pathways, their variations, and how they eventually join to form the AW boundary current (AWBC) remain unclear in the area because of the lack of in situ measurements (Koenig et al., 2017b; Menze et al., 2019; Meyer et al., 2017).

Along its paths, the AW is cooled and freshened through ice-melt, heat loss to the atmosphere and mixing with shelf waters (Boyd & D’Asaro, 1994; Fer et al., 2020; Onarheim et al., 2014; Renner et al., 2018; Rudels et al., 2015). In the Western Nansen Basin (WNB) in particular, deep winter mixed layers reaching 500 m (V. Ivanov et al., 2018; Pérez-Hernández et al., 2019), exchanges with fjords west of Svalbard (Koenig et al., 2018) and troughs outflows from the Barents Sea (Athanasé et al., 2020; Schauer et al., 1997) contribute to alter AW properties. The rather unstable AWBC has been observed to shed AW eddies, further contributing to the erosion of AW properties over the slope (Athanasé et al., 2019; Pérez-Hernández et al., 2017; Våge et al., 2016).

Several studies pointed out to the development of a more energetic ocean state under a declining sea-ice cover (Polyakov et al., 2017, 2020; Timmermans & Marshall, 2020). Polyakov et al. (2020) documented an intensification of current velocities in the upper 50 m of the eastern Eurasian Basin between 2004 and 2018 (by about 20%), associated with an enhanced coupling between winds and the increasingly ice-free ocean. Recent observations north of Svalbard suggested previously unnoticed circulation patterns (Kolås et al., 2020). As observations require substantial resources and efforts and remain scarce in the Arctic, models can be useful to investigate possible changes in circulation and currents.

The 1/12° Mercator Ocean operational physical system, called PSY4 hereafter, has shown some skills in reproducing the hydrography, mesoscale structures and seasonal signals in the upper Western Eurasian Basin (Athanasé et al., 2019, 2020; Bertosio et al., 2020; Koenig et al., 2017b, 2017a). PSY4 model fields covering 14 years (2007–2020) documented interannual variations of deep winter mixed layers in the WNB, and several processes at stake in modifying AW properties (Athanasé et al., 2020). A major change was observed in 2011, with the emergence of new “Marginal Convection Zones” (northern Yermak Plateau, Sofia Deep and continental slope) exhibiting from then on, occasional ice-free conditions and intense winter convection events.

The objective here is to use the PSY4 system to examine the circulation of AW in the WNB over 2007–2020 in this context of rapid Arctic changes. We examine and quantify the evolution of AW characteristics and pathways across the Yermak Plateau, on the continental slope and its vicinity, on seasonal and interannual time scales. This study is structured as follows. Section 2 introduces the Mercator Ocean operational system and reminds the model strengths and limitations. Further model evaluation includes comparisons with new unpublished data. Section 3 revisits the mean and seasonal AW circulation and volume transports in the WNB, while Section 4 focuses on interannual variations over 2008–2020. Section 5 examines the 12-year trends in water properties and circulation in the upper 1,000 m of the WNB. Results are summarized and discussed in Section 6.

2. The PSY4 System: Performance and Limitations

2.1. The Mercator Ocean Operational System (PSY4)

In the frame of Copernicus Marine Environment Monitoring Service (CMEMS; <http://marine.copernicus.eu/>) Mercator Ocean delivers the high resolution 1/12° global operational PSY4 system since October 2006 (Lellouche et al., 2018). Forcings and data assimilation in the Arctic region are summarized in Athanase et al. (2020). The model component is based on the NEMO ocean model, with a 1/12° ORCA grid type (i.e., daily outputs with horizontal resolution of 4 km in the WNB; Hu et al., 2019). The water column is composed of 50 vertical levels, with typically 1 m resolution at the surface decreasing to 450 m at the bottom and 22 levels within the upper 100 m. When oceans are ice-covered, only sea ice concentration is assimilated. This is in stark contrast with the open ocean regions, where PSY4 assimilates along-track satellite altimetry sea level anomalies, sea surface temperature and in situ vertical profiles of temperature and salinity. The PSY4 system starts in October 2006 from a “cold” start (initial currents are null) using initial climatological conditions from EN4.2.1 hydrographic temperature and salinity data (Good et al., 2013). Here, the first 15 months were considered as a spin-up period in the WNB (see appendix). Hence, daily outputs from April 2008 to May 2020 are used in this study, carefully avoiding the estimated spin-up period.

An extensive evaluation of PSY4 in the WNB was performed in Athanase et al. (2020), using nearly 1,500 independent in situ temperature-salinity profiles and mooring data in the AWBC (1-year long, at 30°E) and in the WSC (5-years long). PSY4 represented a realistic AW inflow and well reproduced hydrographic properties, in spite of some inherent limitations that one should bear in mind. Indeed, the model resolution is not fully eddy-resolving in the WNB (i.e., grid size of 4 km, and Rossby deformation radius of ~10 km; Crews et al., 2018). Moreover, the model lacks tides which are important on the Yermak Plateau (Koenig et al., 2017a; Padman et al., 1992) and on the shelf (Renner et al., 2018). Finally, the PSY4 bathymetry matched the IBCAO bathymetry (Jakobsson et al., 2012) in the WNB, except for a small region at the Kvitøya Trough opening (see appendix in Athanase et al., 2020).

2.2. Further PSY4 Evaluation: Comparisons With Recent Observations

We took advantage of a newly retrieved 32 months-long time-series of temperature and salinity at 350 m (in the AW layer) from a mooring deployed in the Yermak Pass (from September 2017 to May 2020; yellow stars in Figure 1; Labaste et al., 2020) to evaluate PSY4 in the recent years. The mooring was located in a region of rather large mean gradients and large standard deviations (STDs) (Figures 2a and 2c). The colocalized PSY4 temperature and salinity well reproduced the mean and variations of the 10-days smoothed in situ time-series (Figures 2b and 2d). PSY4 was on average 0.3°C warmer (respectively, 2.9°C and 2.6°C) and 0.03 g/kg saltier (respectively 35.18 and 35.15 g/kg) than observations at this location. Model STDs were on the same order as those of the 10-days smoothed observations (0.4°C and 0.03 g/kg). Variations were correlated at the 99% significance level ($r = 0.68$).

We also compared PSY4 sea surface height (SSH) to satellite SSH from a multi-mission altimetry product prototype for the Arctic Ocean (nonassimilated in PSY4), available from July 2016 to June 2018. The satellite product is based on the combination of measurements from three altimeters (SARAL/AltiKa, CryoSat-2, and Sentinel-3A) through an optimal interpolation scheme (Bretherton et al., 1976; Ducet et al., 2000). A

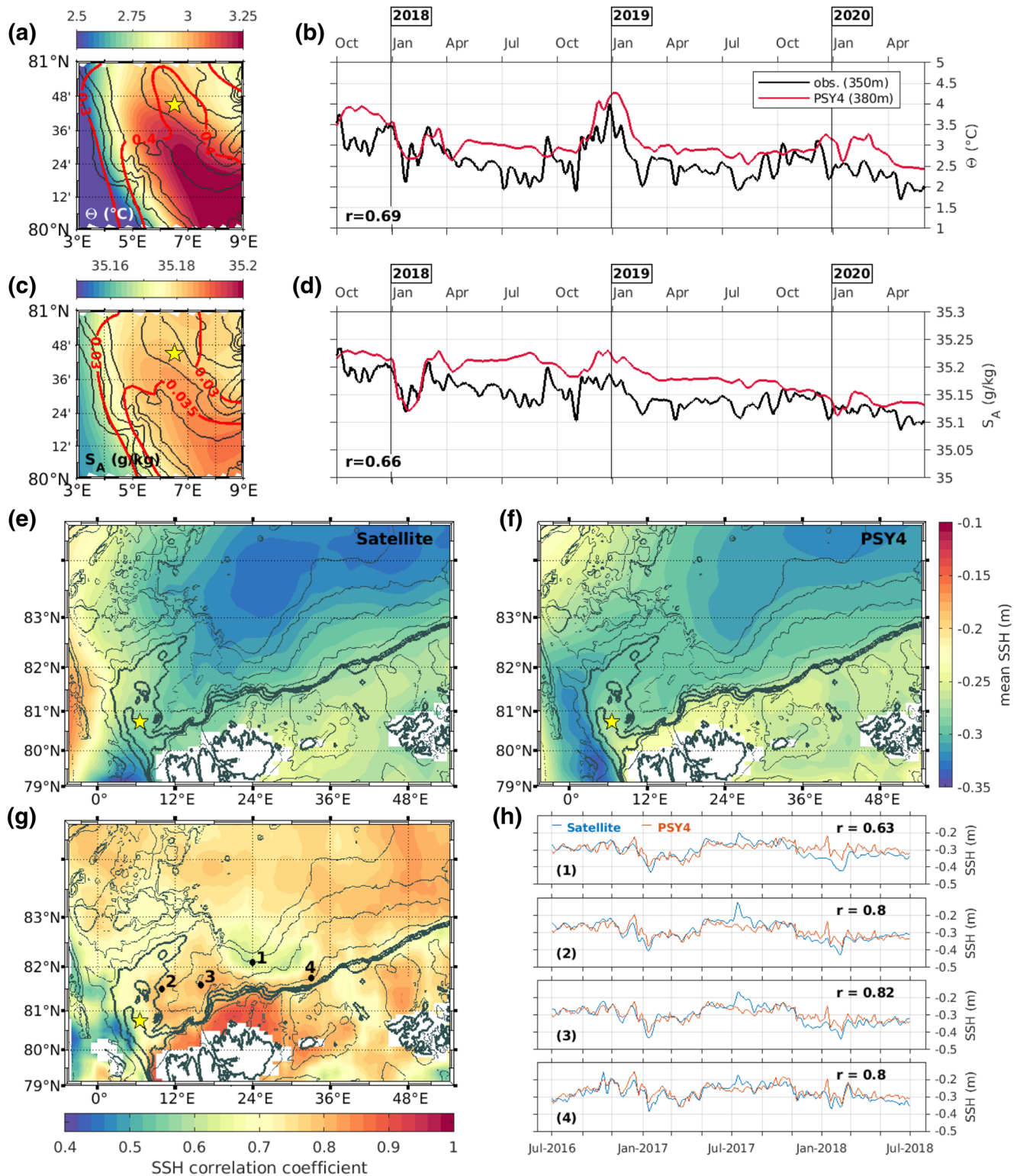


Figure 2. (a) Map of PSY4 Conservative Temperature (Θ , $^{\circ}\text{C}$) at 380 m averaged over October 2016–May 2020. Isobaths are plotted every 100 m from 500 to 1,000 m. Red lines delineate contours of STDs over the same period. The yellow star is the location of the mooring as in Figure 1. (b) 10-days smoothed time-series of Θ ($^{\circ}\text{C}$) from the mooring SBE at 350m (black curve) and from PSY4 at 380 m, that is, the closest vertical level available. (c and d) same for Absolute Salinity (S_A , g/kg). (e) Mean sea surface height (SSH, m) from the CNES/CLS satellite altimetry prototype product over July 2016–June 2018. (f) Mean SSH (m) from PSY4 over the same period and degraded to the same temporal resolution (3 days). Both the PSY4 and satellite-derived SSH were interpolated on a regular grid (horizontal grid spacing 0.1° in latitude, 1° in longitude). (g) Correlation coefficients between the SSH time-series at each point. Examples of SSH time-series at the points 1 to 4 in (g) are presented in (h).

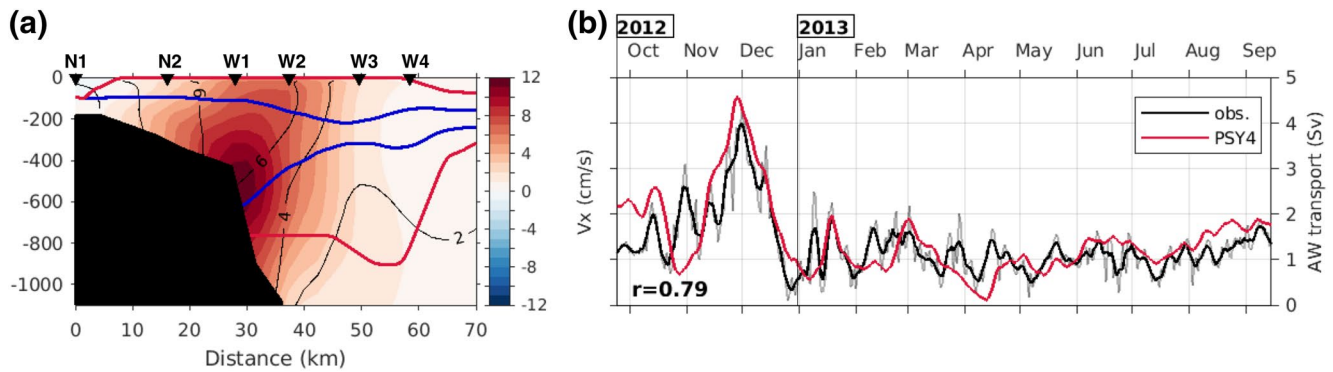


Figure 3. (a) Average cross-section velocity (V_x , cm/s) at the A-TWAIN mooring array (pink stars in Figure 1), between September 2012 and September 2013 (A-TWAIN acquisition period). Black contours are the associated V_x STDs (2, 4, and 6 cm/s). Blue and red lines delineate respectively the minimal and maximal AW layer vertical extent during the period. Black markers N (W) are moorings deployed by the Norwegian Polar Institute (Woods Hole Oceanographic Institution). (b) 10-days smoothed Atlantic Water (defined as $\Theta > 1^\circ\text{C}$, $S_A > 35.05$ g/kg) volume transport at the A-TWAIN mooring array in the 100–1,200 m layer, from mooring data (thick black) and PSY4 (red). The thin black line is the daily in situ AW transport.

dedicated low level processing (Poisson et al., 2018) of altimeter waveforms ensures consistency between open ocean and ice covered areas of the Arctic Ocean. This satellite product provides sea level anomaly (SLA) and absolute dynamic topography (ADT) fields on a 25 km grid every 3 days for latitudes greater than 50°N . The product is freely available from AVISO (<https://www.aviso.altimetry.fr/en/data/index.php?id=3438>) along with a detailed description of the processing (https://www.aviso.altimetry.fr/fileadmin/documents/data/tools/gridded_sla_arctic_multimission.pdf).

The SSH mean fields exhibited similar patterns in both the PSY4 and the satellite-derived products, with larger values in the Transpolar Drift, on the shelf and slope than in WNB interior (Figures 2e and 2f). In particular, they both exhibited low SSH values north of the 3,800 m isobath (Figure 1) east of 15°E (Figures 2e and 2f). The PSY4 and satellite-derived SSH were well correlated, with correlation coefficients always above 0.5 in the WNB area (significant to the 95% confidence level; Figure 2g). Significant correlations were above 0.7 north of Svalbard, along the continental slope and in the basin interior, and were the lowest, yet still around 0.45–0.6, west of Yermak Plateau and near 24°E – 82°N (Figures 2g and 2h).

2.3. AW Volume Transport at 30°E : PSY4 Performance

Following the TEOS-10 (Thermodynamic Equations of Seawater) international standard (e.g., Valladares et al., 2011), Absolute Salinity S_A (g/kg) and Conservative Temperature Θ ($^\circ\text{C}$) are used in this study.

The PSY4 performance in reproducing the mean and variations of AW properties was previously assessed at the A-TWAIN mooring array (30°E , purple stars in Figure 1) in Athanase et al. (2020). Here, we compared modeled and observed AW volume transports across the A-TWAIN section from September 2012 to September 2013. At this location, the boundary current intensity was variable (Figure 3a), and the AW layer had vertical extents ranging from the upper 800 m of the water column (red contours in Figure 3a) to about 200 m in the 200–400 m layer (blue contours in Figure 3a). The AW layer was defined here as $\Theta > 1^\circ\text{C}$, $S_A > 35.05$ g/kg (corresponding to a potential density always larger than 27.6 kg/m³ in PSY4), as in Pérez-Hernández et al. (2019). Pérez-Hernández et al. (2019) computed geostrophic AW volume transport taking into account only positive (eastward) across-section velocities in the 100–1,200 m layer (black line in Figure 3b). AW volume transport from PSY4 (same water mass criteria) was computed over the 100–1,200 m layer (red line in Figure 3b). The model AW volume transport in the upper 100 m was close to zero (mean of 0.07 Sv, STD of 0.1 Sv). The PSY4 AW transports closely followed the 10-day smoothed observed one. Observations and PSY4 had respective means of 1.3 and 1.5 Sv, STDs of 0.7 and 0.8 Sv, with a correlation coefficient of $r = 0.79$ significant at the 99% confidence level. The model only seldomly missed peaks in volume transport (as in November 2012 and January 2013). We now use the model to further examine AW transport in the WNB.

3. AW Circulation and Volume Transport: Means and Seasonal Variations Over 12 Years

North of Svalbard, the AW heat maintains the Whalers' Bay ice free year-round (Figure 4a; Onarheim et al., 2014), despite the northerly winds which tend to push sea-ice into the area (Figures 4a and 4b). The WSC, reaching the Yermak Plateau, splits into the Yermak Branch, Yermak Pass Branch, and Svalbard Branch (Figures 1, 4c, and 4d). The upper part of the AW layer, cooling and freshening through sea-ice melt and heat loss to the atmosphere, is transformed into a less dense surface layer (Rudels et al., 2015; Figures 4e–4h). On average, the AW signature at 265 m could be found as far offshore as the 3,900 isobath (red contours in Figures 4e and 4g). Near the surface the AW mean horizontal extent was reduced to the southern Yermak Plateau and the slope west of 11°E (red contours in Figures 4f and 4h).

As in Koenig et al. (2017a), we used the PSY4 system to investigate the partition of the AW flow downstream of the WSC. We examined the AW volume transport across 13 sections near the Yermak Plateau and in the WNB (Table 1; Figure 5; WSC); Svalbard Branch (SB); Yermak Pass Branch (YPB); Yermak Branch (YB); Return Yermak Branch (RYB); at the A-TWAIN mooring location in the boundary current; AW Boundary Current Sections 1 to 4 (AWBC 1 to 4); Offshore Section 1 (OS1) and Offshore Section 2 (OS2). Note that sections in the WSC, SB, and YPB are identical to Koenig et al. (2017a), extending the time-series until 2020. The remaining sections complement the analysis further east. To ensure we capture all recirculations over the Plateau, an additional longer section (noted YP) was taken along the axis of the Yermak Plateau.

AW volume transports were computed following two methods: net transport as in Koenig et al. (2017a), and taking into account only positive cross-section velocities as in Pérez-Hernández et al. (2019). The net transport was on average 25% lower over the Yermak Plateau and 5% lower near the continental slope (Table 1), yet time-series were highly correlated (with $r > 0.9$ for all 13 sections, significant to the 99.9% level). Transports shown hereafter were estimated using only positive cross-section velocities. Two AW definitions were used ($\Theta > 1^\circ\text{C}$, $S_A > 35.05$ g/kg as in Pérez-Hernández et al., 2019 –shown hereafter–, and $\Theta > 1.5^\circ\text{C}$ as in Koenig et al., 2017a). The two definitions provided similar results (see supporting information S1).

3.1. AW Volume Transport Across and Around Yermak Plateau

The AW carried by the modeled WSC ranged from 1.5 to 7 Sv, with a mean of 4 Sv and STD of 1.5 Sv, and exhibiting large seasonal variations (red curve in Figures 5b and 6a). Maximum values of AW volume transport in the WSC were reached on average in January (5.2 Sv, Table 1) and were minimal in July (2.9 Sv, Table 1).

The modeled YPB constituted the main path for AW over Yermak Plateau with an AW volume transport of 1.2 ± 0.8 Sv (mean \pm STD), which was largely correlated with the WSC AW transport over the 2008–2020 period ($r = 0.78$) and exhibited the same seasonal variations (Table 1, blue curve in Figures 5b, 6a, 6c, and 6d). In summer, AW transport in the YPB was on the same order as in the SB (in agreement with Menze et al., 2019). The SB carried a smaller volume of AW on average (0.6 ± 0.3 Sv), showed marginal seasonality (maximum in January of about 0.7 Sv, minimum in July of about 0.5 Sv) and a smaller correlation to the WSC AW transport ($r = 0.48$; green curve in Figures 5b and 6a).

The mean modeled YB carried some AW along the western flank of Yermak Plateau, losing AW to westward recirculations (Figure 4c). As a result, the AW volume transport was 0.5 ± 0.4 in the YB at 82°N on average (Table 1). Past 82°N, the YB flow either continued along the western edge of the Yermak Plateau or crossed over the Plateau (Figure 4c). Along the eastern flank of the Plateau, a southward flow at 81.5°N was called the RYB, being essentially fed by the YB ($r = 0.63$ between YB and RYB). The RYB carried about 0.3 ± 0.25 Sv, representing 70% of the YB AW volume transport (Table 1, Figures 5a and 5b). These branches (YB and RYB) exhibited no seasonal variations (brown and yellow curves in Figures 6a, 6c, and 6d) and little correlation with the WSC AW transport ($r = 0.31$, yet significant at the 90% confidence level).

The sum of AW volume transports across the YPB, SB, and YB at 82°N (mean of 2.2 Sv, STD of 1.1 Sv) corresponded to the net AW volume transport across YP (mean of 2.2 Sv, STD of 1.2 Sv) and to about 55% of the AW volume transport from the WSC section (Table 1). This implies that about 45% (1.7 Sv on average) of the modeled WSC AW inflow recirculated toward Fram Strait south of 82°N (AW transport from recirculation branches noted rB, gray curve in Figure 5b).

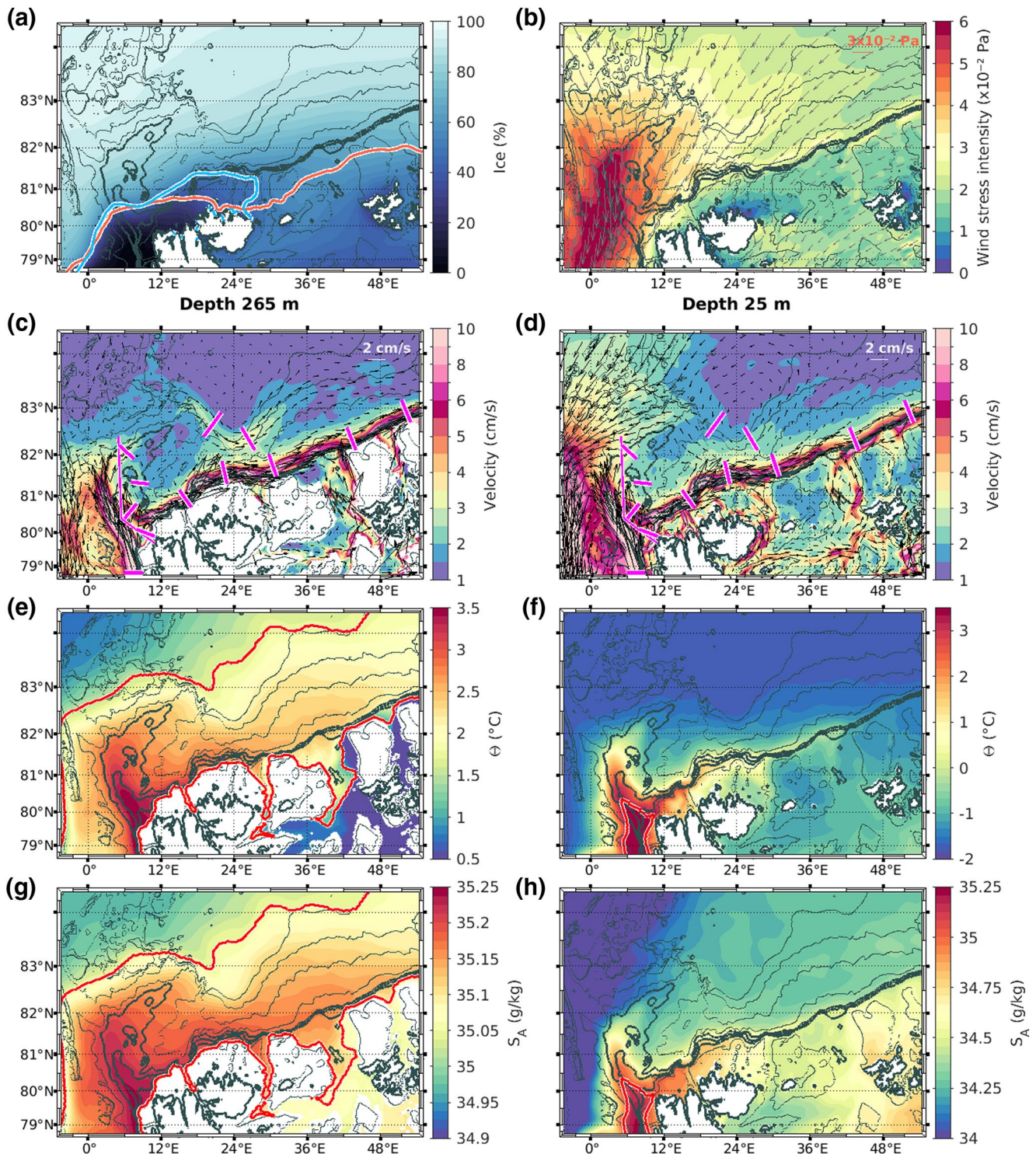


Figure 4. Mean PSY4 fields over 2008–2020 in the Western Nansen Basin. (a) Mean ice concentration (%). Orange and blue solid contours are respectively the mean July and January ice edge (40% ice concentration). (b) Mean wind stress (Pa, gray arrows), with intensity in background color. (c) Mean velocity vectors (black arrows) and intensity (color, cm/s) at 265 m and (d) 25 m. Magenta sections are used for AW volume transport computations. (e) Mean Conservative Temperature (θ , °C) at 265 m and (f) 25 m. (g–h) Same for Absolute Salinity (S_A , g/kg). Red contours delineate the horizontal limit of Atlantic Water (such as $\theta > 1^\circ\text{C}$ and $S_A > 35.05$ g/kg) at 265 and 25 m. Isobaths 500, 700, 1,000 m are in thick lines, 200, 2,000, 3,400, 3,800 and 3,900 m in thin lines.

Table 1
Statistics of the AW Volume Transport (Sv) in 2008–2020 Across 13 Sections Near the Yermak Plateau and in the Western Nansen Basin, Marked (and Colored) in Figure 5

Section	Mean	STD	January		July	
			Mean	Min/Max	Mean	Min/Max
WSC	4.0 (3.8)	1.5 (1.6)	5.2 (4.9)	1.7/9.7	2.9 (2.5)	1.0/4.5
YP	2.95 (2.2)	1.2 (1.2)	3.8 (3.1)	1.0/7.85	2.0 (1.3)	0.5/3.6
SB	0.6 (0.45)	0.3 (0.4)	0.7 (0.6)	0.0/2.1	0.5 (0.5)	0.1/1.1
YPB	1.2 (1.0)	0.8 (0.9)	1.75 (1.6)	0.0/5.1	0.5 (0.3)	0.0/1.3
YB	0.5 (0.4)	0.4 (0.4)	0.45 (0.4)	0.0/1.8	0.4 (0.3)	0.0/1.5
RYB	0.3 (0.2)	0.25 (0.3)	0.3 (0.2)	0.0/1.3	0.3 (0.2)	0.0/0.8
AWBC1	1.9 (1.8)	1.1 (1.1)	2.9 (2.7)	0.6/6.1	1.0 (0.9)	0.0/2.6
AWBC2	1.8 (1.7)	1.0 (1.1)	2.6 (2.4)	0.6/5.6	1.0 (0.9)	0.1/2.0
A-TWAIN	1.6 (1.4)	0.9 (1.0)	2.3 (2.2)	0.3/5.7	1.0 (0.75)	0.2/2.05
AWBC3	1.3 (1.2)	0.8 (0.85)	1.9 (1.8)	0.3/4.6	0.65 (0.5)	0.0/1.55
AWBC4	1.25 (1.2)	0.8 (0.8)	1.9 (1.8)	0.0/4.7	0.65 (0.6)	0.1/1.6
OS1	0.3 (0.3)	0.3 (0.3)	0.4 (0.3)	0.0/1.3	0.3 (0.3)	0.0/0.9
OS2	0.6 (0.5)	0.3 (0.3)	0.5 (0.5)	0.0/1.2	0.5 (0.4)	0.1/1.4

AW is defined as $\Theta > 1^\circ\text{C}$, $S_A > 35.05$ g/kg. Only positive cross-section velocities are considered (as indicated by the mean flow in Figure 4c). Values in italics and parentheses are for net AW volume transports. Section names are as in Figure 5.

3.2. AW Progression Downstream of Yermak Plateau

3.2.1. AW Boundary Current

The AW transport at the AWBC1 section (16°E ; 1.9 Sv) was on average 5% larger than –and very correlated ($r = 0.88$) with– the sum of the AW transports of YPB and SB. This suggested that to the first order, the AW boundary current was mainly fed by these two branches. The complex and rather weak recirculations in the Sofia Deep (Figures 4c and 4d) were therefore minor contributors to the boundary current. Along the continental slope, the AW volume transport diminished eastward, with 1.9 ± 1.1 Sv at 16°E (mean \pm STD), 1.8 ± 1.0 Sv at 23°E , 1.6 ± 0.9 Sv at the A-TWAIN location (30°E), to reach a value of about 1.3 ± 0.8 Sv at 43°E and 52°E (Table 1, gray and pink curves in Figures 5c and 6b). On average, the largest AW volume transport reductions occurred between 23°E and 43°E (Table 1). In this area, processes have potential to reduce the AW volume transport, with the meandering and shedding of eddies, and deep convection in winter transforming AW into halocline water (Athanasé et al., 2020; V. Ivanov et al., 2018). As in the WSC, YPB, and SB, seasonal variations in AW volume transport were large in the AWBC (amplitude ~ 2 Sv), with maximum values reached on average in January and minimum values in July (Table 1, Figure 6a compared to Figures 6b, 6c, and 6d). The daily AW volume transports across the five sections in the boundary current were highly correlated, with correlation coefficients to AWBC1 (16°E) decreasing from $r = 0.9$ at AWBC2 (23°E) to $r = 0.8$ at AWBC4 (52°E ; Figure 5c).

3.2.2. Offshore Circulation

At 265 m, the mean velocity fields highlighted an offshore “V-shaped” circulation pattern straddling the 3,800–3,900 m isobaths (Figures 1 and 4c), with its southernmost extremity located near 82°N , 24°E (mean velocities larger than 3 cm/s in Figures 4c and 4d). The offshore circulation followed the large lateral gradients of temperature and salinity (and thus density; Figures 4c, 4e, and 4g).

The western part of the V-shaped circulation consisted in a southeastward current carrying some AW (mean of 0.3 ± 0.3 Sv; Table 1 and purple lines in Figure 5c). On the mean, this current straddled the 35.1 g/kg and 2°C isolines (Figures 4f and 4h). The northeastward flow following 3,800–3,900 m isobaths, that is, eastern part of the V-shaped offshore circulation, carried on average 0.6 ± 0.3 Sv of AW (Figures 4c and 4d and blue

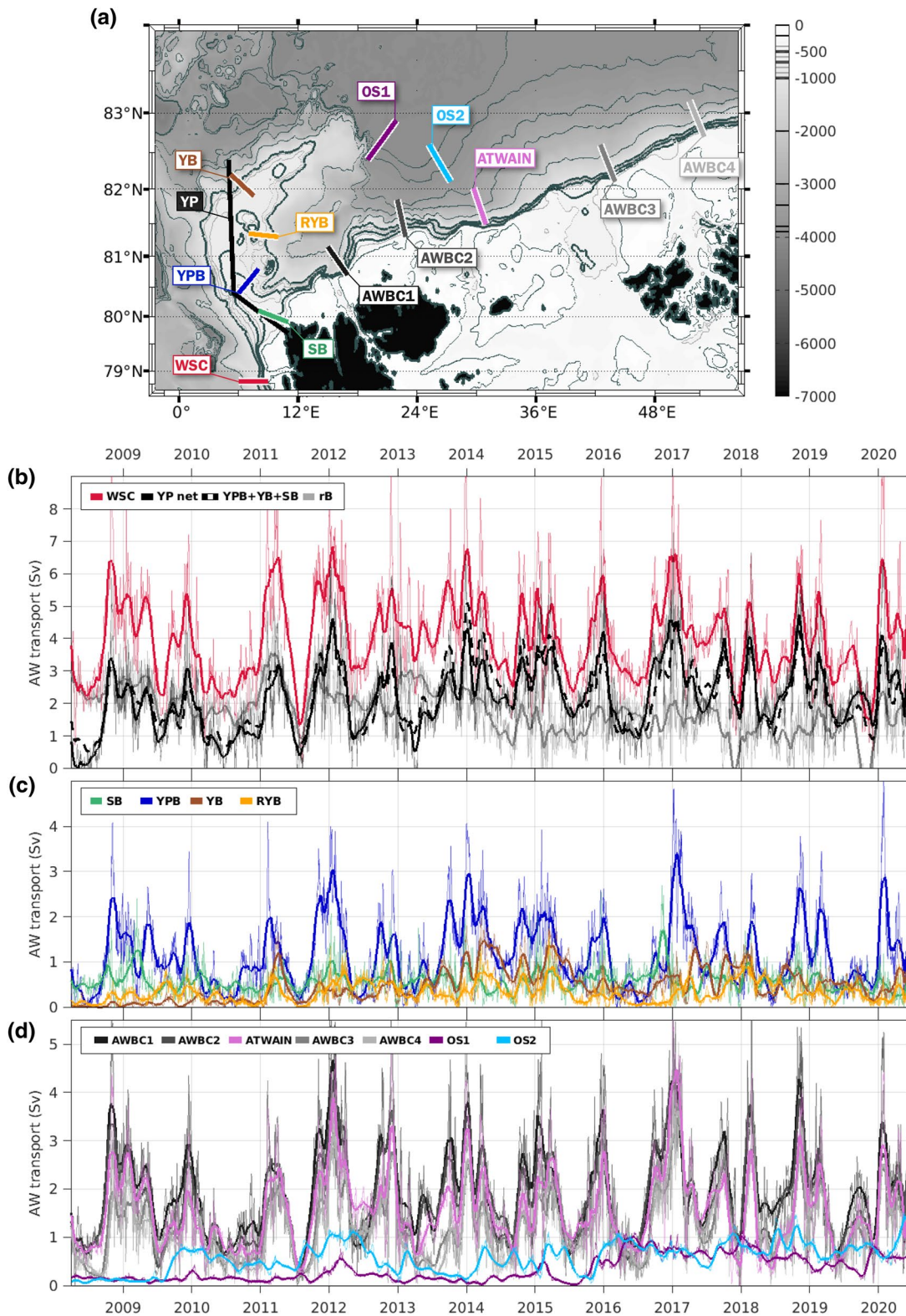


Figure 5. (a) Location of the 13 sections across which Atlantic Water (such as $\Theta > 1^\circ\text{C}$, $S_A > 35.05 \text{ g/kg}$) volume transports were computed and presented in Table 1. A-TWAIN, mooring array at 30°E ; AWBC, Atlantic Water Boundary Current; OS1 and OS2, Offshore Sections 1 and 2; RYB, Return Yermak Branch; SB, Svalbard Branch; WSC, West Spitsbergen Current; YB, Yermak Branch; YP, Yermak Plateau; YPB, Yermak Pass Branch. (b) Time-series of AW volume transports (Sv) between April 2008 and May 2020 for the WSC, AW crossing the Plateau (YP net; sum of YPB, YB, and SB) and recirculation branches (rB, computed as WSC – YP net). (c) Same for sections located over the Yermak Plateau. (d) Same for sections located downstream of Yermak Plateau.

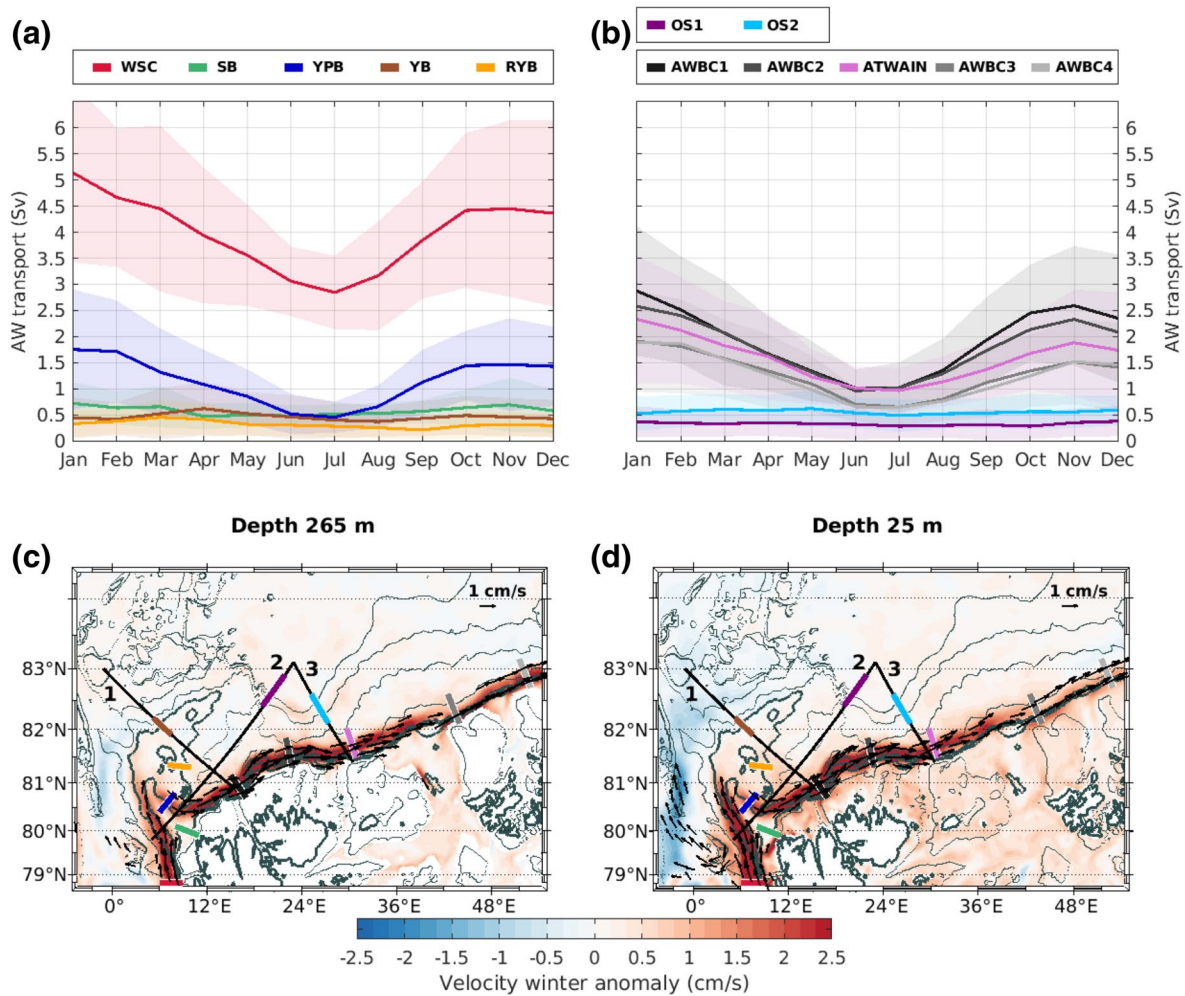


Figure 6. (a) Monthly means of AW volume transport (Sv) across the 5 sections over Yermak Plateau, in 2008–2020. (b) Monthly means of AW volume transport (Sv) across the 7 sections downstream of Yermak Plateau, in 2008–2020. Shaded envelopes in (a) and (b) are interannual STDs for each month. (c) Winter velocity anomaly (cm/s) (with respect to the 12-years mean) at 265 m and (d) 25 m. Winter is defined at the October-to-March period. Seasonal velocity anomaly vectors are plotted in black arrows for velocity anomalies larger than 1 cm/s. Sections names and color codes are as in Figure 5. Transects 1, 2, and 3 are shown in Figures 7, 9, and 10.

lines in Figure 5c). Concurrently, relatively warm and salty AW ($\Theta > 2^{\circ}\text{C}$, $S_A > 35.1$ g/kg) spread offshore east of 24°E , following the bulk of the isobaths, suggesting that part of the boundary current AW may be advected by this northeastward flow (Figures 4e and 4g). In contrast with the continental slope, this off-shore circulation exhibited no seasonal variations in AW volume transport (Table 1, purple and blue lines in Figure 6b) and in velocity (Figures 6c and 6d). Interestingly, time-series of AW volume transport suggested a development of the V-shaped circulation in winter 2009 for the eastern part (blue line in Figure 5c) and in 2016 for the western part after a peak in 2012 (purple line in Figure 5c).

4. Interannual Variations of AW Volume Transport

Time-series of AW volume transport across the 13 sections in the WNB exhibited large variations on interannual time scales (Figure 5). To investigate further interannual variations we examined the evolution of properties and velocities along three transects (Figures 6c–6d): one encompassing the YB and AWBC1 sections and crossing the northern part of Yermak Plateau (transect 1, Figure 7), and two from the slope offshore. Transect 2 comprised OS1 and YPB sections while transect 3 extended from the A-TWAIN section out to 83°N across OS2 (Figures 9 and 10). Linear trends were estimated over the time span of available

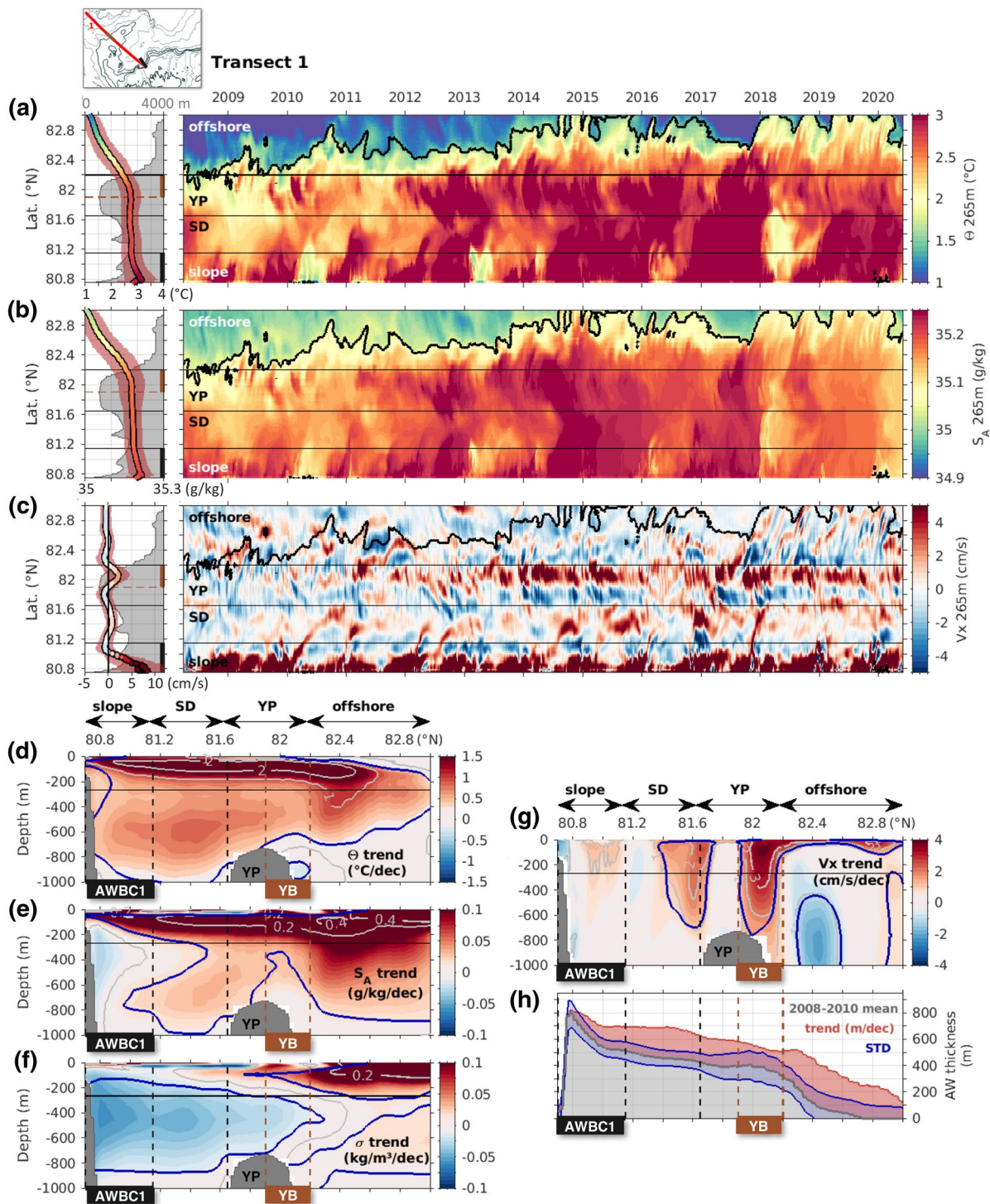


Figure 7. (a) Conservative Temperature (Θ , °C) at 265 m along transect 1 (shown in the insert), (left) mean and STD (shaded envelope) in 2008–2020, with bathymetry in shaded gray, and (right) daily resolution. Same for (b) Absolute Salinity (S_A , g/kg) and (c) cross-section velocity (V_x positive when directed northeastward, cm/s). Main geographical features are delineated with horizontal lines. Thick black contours delineate AW ($\Theta > 1^\circ\text{C}$ and $S_A > 35.05$ g/kg). (d) Linear trend in Conservative Temperature (Θ , °C/decade) along transect 1 (0–1,000 m), computed over 2008–2020. (e) Same in Absolute Salinity (S_A , g/kg/decade), (f) in potential density (σ , kg/m³/decade) and (g) cross-section velocity (V_x , cm/s/decade). Gray contours are decadal trend isolines. Blue contours on (d–g) delineate areas where the 12-years trend is larger than the STD. (h) AW layer thickness along transect 1, 2008–2010 mean (gray area, m), 12-years STD (blue envelope centered on the 2008–2010 mean, m) and linear trend (red area, m/decade) added to the 2008–2010 mean. The horizontal line indicates the 265 m level shown in (a–c), vertical lines delineate geographic regions as reported below. SD, Sofia Deep; YP, Yermak Plateau. AWBC1 and YB (Yermak Branch) as in Figure 5.

model fields (12 years, 2008–2020) and compared to STD values (of detrended time-series) (panels d–h in Figures 7, 9, 10, 12 and 13). An animation of PSY4 mapped velocity fields at 265 m over 2008–2020 with a 3-days temporal resolution is provided in supporting information (S2).

4.1. Interannual Variations in AW Volume Transport Across and Around Yermak Plateau

4.1.1. Strengthening of the YB

A striking feature in transect 1 was the strengthening of the YB at 82°N on the western flank of Yermak Plateau, with larger northeastward velocities at 265 m from 2011 onwards (Figure 7c) and warmer and saltier waters (Figures 7a and 7b). Vertical sections along transect 1 illustrated these YB changes throughout the upper 1,000 m of the water column, with a large increase in AW layer thickness (up to +150 m/decade, Figure 7h) and in cross-section velocities down to the seafloor (Figure 7g). Velocity trends reached 3.5 cm/s/decade near the surface. The temperature and salinity trends in the YB were large in the upper 200 m with values of +2°C/decade and +0.2 g/kg/decade (Figures 7d and 7e).

Positive trends in velocity and AW thickness led to an increased AW volume transport across the YB section (mean of 0.2 Sv in 2008–2012 and 0.7 Sv in 2013–2020, brown bars in Figure 8b). AW transport through the YB at 82°N was the largest in 2014/2015 (annual mean of 0.9 Sv), making up for 23% of the WSC AW transport (compared to 12% on average over 2008–2020) (Figure 8b). That year, the net AW volume transport across the Yermak Plateau accounted for 70% of the WSC transport (YP, black bars in Figure 8a). In other words, in 2014/2015 only 30% of the AW volume carried by the WSC recirculated toward Fram Strait south of 82°N instead of 45% on average (rB, gray bars in Figure 8a). The year 2014/2015 also corresponded to a clear decline of the AW volume recirculating toward Fram Strait south of 82°N, from a mean of ~2.2 Sv in 2008–2013 (i.e., 55% of the WSC), to ~1.3 Sv from 2014 onwards (i.e., 32% of the WSC) (gray bars in Figure 8a).

4.1.2. Contrasting Variations of the YPB and SB

Waters in the YPB became progressively warmer and saltier (Figures 9a and 9b), with a substantial increase near the surface (+2°C/decade, +0.2 g/kg/decade), while below 100 m they became lighter by about -0.05 kg/m³/decade as a result of warming (+0.5°C/decade) and freshening (-0.05 g/kg/decade) (Figures 9d–9f). Positive trends in velocity (+2 cm/s/decade) and AW thickness (+150 m/decade) were centered over the lower slope (900 m isobath, Figures 9g and 9h), suggesting a slight displacement of the core of the YPB to deeper isobaths. However, the velocity trends were small compared to the large STDs in the YPB (STD of 5 cm/s at 265 m, for a mean of 5 cm/s, Figure 9c). This variable YPB flow, with seldom occurrences of northwestward velocities ($V_x < 0$ in summer 2016 for example; cf. Koenig et al., 2017a) (Figure 9c) was consistent with previous studies (Koenig et al., 2017a; Menze et al., 2019).

The resulting interannual variations in AW volume transport through YPB were large, ranging from 0.8 Sv in 2012–2013 (20% of the WSC AW transport) to 1.7 Sv in 2013–2014 (34% of the WSC AW transport; blue bars in Figure 8b). In contrast with the YPB, the SB exhibited little variations in AW volume transport (0.4–0.65 Sv, representing 11%–17% of the WSC transport, green bars in Figure 8b).

4.1.3. Intensification of the Circulation in the Sofia Deep

Transects 1 and 2 also provided information on the relatively small and variable velocities in the Sofia Deep (mean $V_x \sim 2$ cm/s, STDs of about 2–3 cm/s, Figures 7c and 9c). At 265 m, these velocities resulted in a mean flow predominantly southward along the eastern flank of the Yermak Plateau (centered around 81.8°N) and in a mean anticyclonic circulation in the Sofia Deep (velocities of 1–2 cm/s; Figures 7c and 9c).

Mirroring the northeastward YB interannual variations (see section 4.1.1), the largest velocities and AW volume transport in the RYB were reached in 2013–2020 (Figures 7c and 8b). These flows (YB pathways and RYB) are schematized with yellow and orange arrows in Figure 14.

The mean anticyclonic circulation in the Sofia Deep consisted of a northeastward flow in the center of the Sofia Deep (near 81.4°N) and a southwestward flow (near 81.1°N) to the north of the eastward boundary current along transect 1 (Figure 7c). This mean anticyclonic circulation showed up in transect 2 as a southeastward flow near 81.4°N, and a northwestward flow near 81.1°N (Figure 9c). Animations of velocity fields

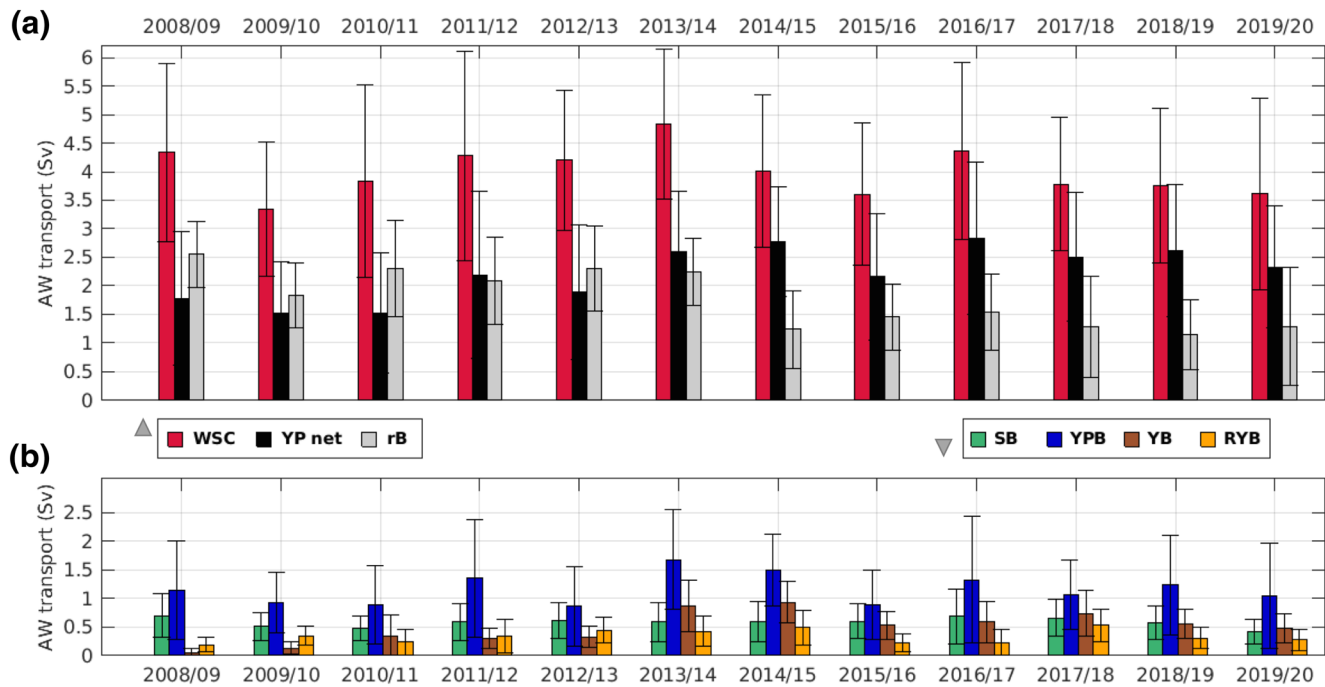


Figure 8. (a) Annual means of AW volume transport in the WSC, AW crossing the Plateau (YP net; sum of YPB, YB and SB) and recirculation branches (rB, computed as WSC – YP net) in 2008–2020. Year-long intervals are taken from June to May of the following year in order to include complete winters. Black bars are STDs for individual years. (b) Same for the 4 sections located over Yermak Plateau. Sections names and color codes are as in Figure 5.

at 265 m (supporting information S2) indicated meanders recurrently detaching from the AWBC near 18°E, where the steep slope abruptly changes direction, contributed to the anticyclonic circulation in the Sofia Deep (Figures 1 and 7c). Meanders either became elongated, following a U-turn anticyclonically (schematized with plain green arrows in Figure 14), or evolved in long-lived slowly-moving AW anticyclonic eddies with rather large radii $R \sim 45$ km (schematized with dashed green arrows in Figure 14). A particularly vigorous and persistent anticyclonic eddy was observed in December 2016, with azimuthal velocities $V_x > 5$ cm/s lasting for over a month (Figures 7 and 9).

The flow in the Sofia Deep evolved from weak and highly variable velocities in 2008–2010 to a recurrent anticyclonic circulation, bringing progressively warmer and saltier waters toward the north from 2010 onwards (Figures 7a–7c, 9a–9c). In the center of the Sofia Deep, trends in northeastward velocities reached +2 cm/s/decade in the upper 600 m (81.4–81.7°N in Figure 7g). The Sofia Deep exhibited large positive trends in temperature and salinity, strongest near the surface (+1°C to +2°C and +0.1 to +0.2 g/kg in the upper 200 m, Figures 9d and 9e) as for the YB, and associated with a mild temperature-driven density decrease below 200 m (-0.03 kg/m³, Figure 9f). This is in agreement with the vertical and lateral progression of AW (thickening about +200 m/decade in the Sofia Deep, Figures 7h and 9h). Notable exceptions to this overall temperature and salinity increase were the seldom occurrences of local and upstream intense winter convection events leading to anomalously cold water at 265 m extending from the slope into the Sofia Deep (February 2013 and 2018, Figures 7a, 7b, 9a and 9b; Athanase et al., 2020).

4.2. Interannual Variations in the Boundary Current Along the Slope

AW volume transport across the boundary current sections was largely correlated with the YPB (Section 3.2.1, Figures 5b and 5c). Shelf-slope and slope-basin exchanges also contributed to modulate AW volume transport across the boundary current sections (AWBC1 to 4 and A-TWAIN, Figures 5c and 11a). For example, exchanges with the Franz-Victoria or Kvitøya troughs contributed to large decreases in annual AW volume transport (e.g., 2018/2019 between AWBC2 and A-TWAIN, 2013/2014 between A-TWAIN and AWBC3, Figure 11a; Athanase et al., 2020). On several occasions, the boundary current was observed meandering along the slope (supporting information S2). In particular, the development of persistent meanders

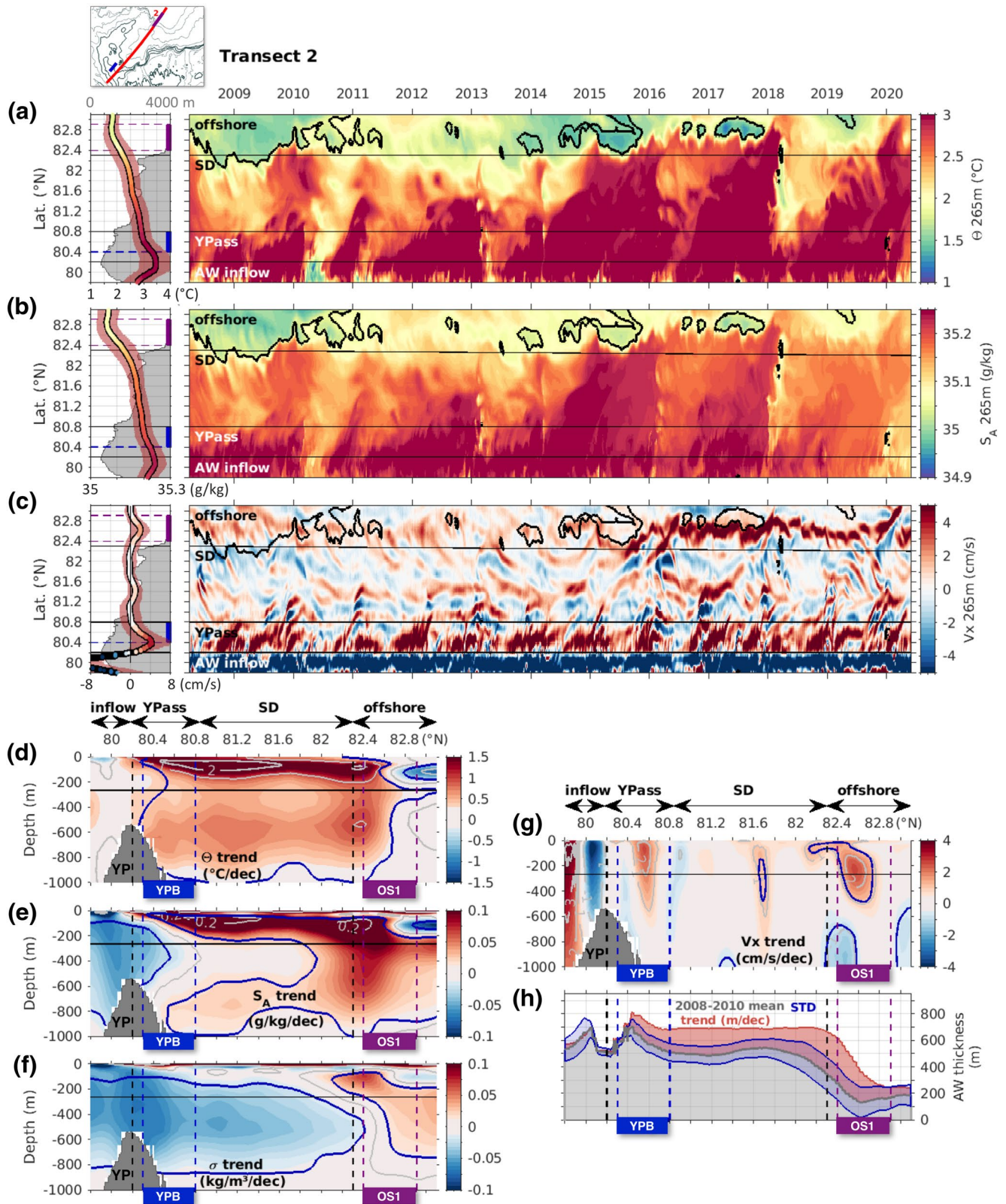


Figure 9. Same as Figure 7, along transect 2. YP, Yermak Plateau; YPass, Yermak Pass; SD, Sofia Deep. YPB, Yermak Pass Branch and OS1, Offshore Section 1 as in Figure 5.

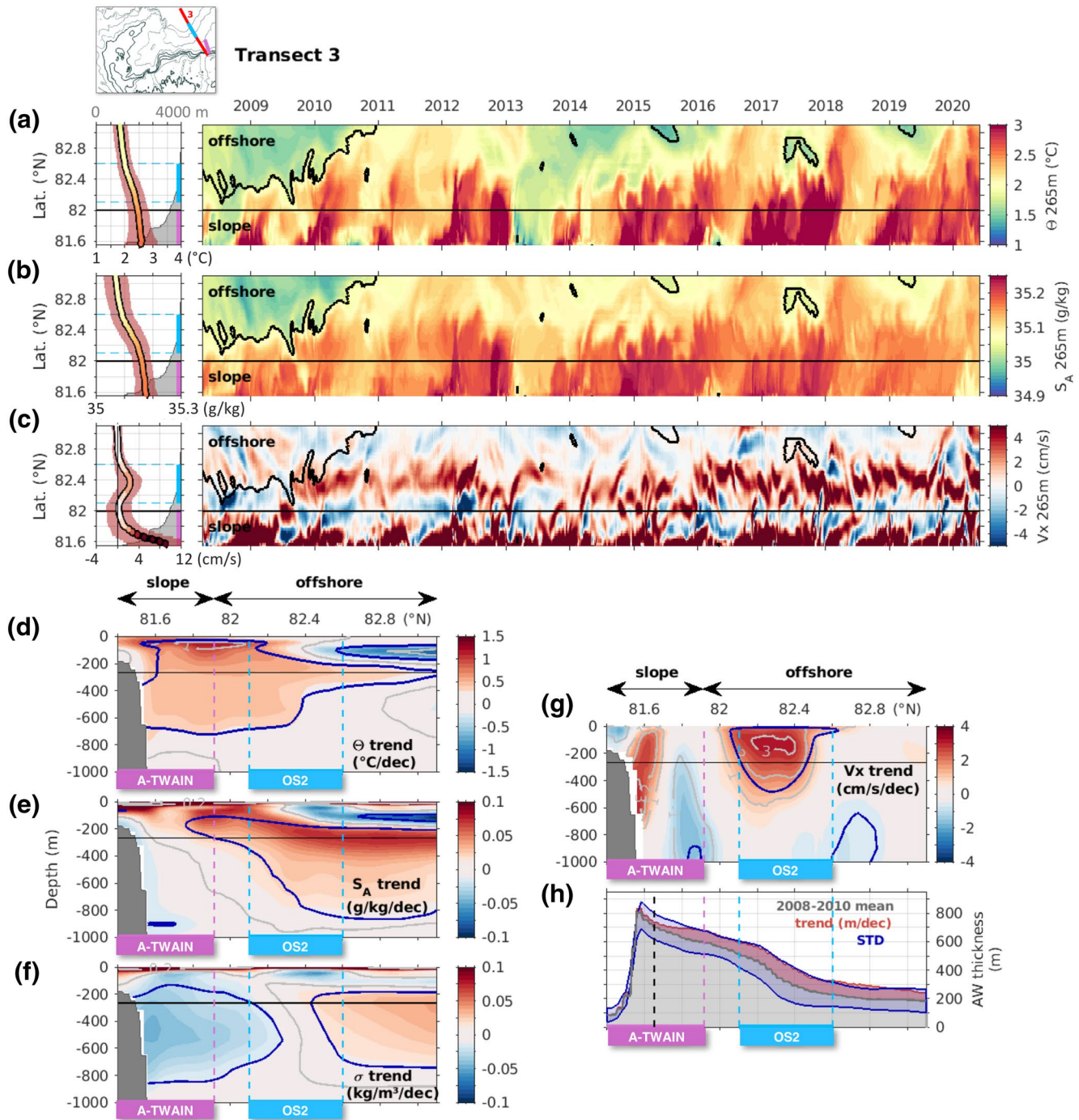


Figure 10. Same as Figure 7, along transect 3. A-TWAIN and OS2 (Offshore Section 2) as in Figure 5.

looping around the AWBC1 section, leaving the shore near 14°E and rejoining the boundary current at the shelf break near 18°E, led to an annual AW volume transport larger at AWBC2 than at AWBC1 (e.g., 2014/2015 and 2016/2017 in Figure 11a; August–October 2014 and February–May 2017 in supporting information S2). In April–May 2012, large eddies detached from the slope between A-TWAIN and AWBC3 to join the offshore circulation at OS2 inducing a drastic decrease in AW volume transport at this location in the boundary current and an increased AW transport at OS2 (Figure 11). Such mesoscale activity between the boundary current and the offshore circulation was common.

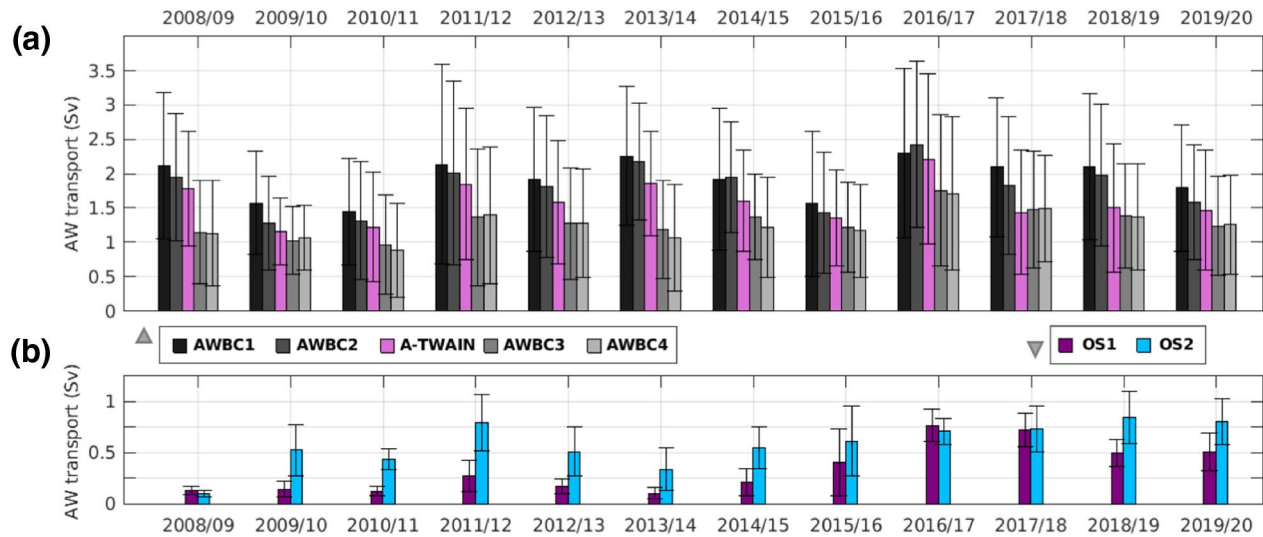


Figure 11. Annual means of AW volume transport (Sv) in 2008–2020, (a) across the 5 sections along the continental slope and (b) at the 2 offshore sections downstream of Yermak Plateau. Year-long intervals are taken from June to May of the following year in order to include complete winters. Black bars are STDs for individual years. Sections names and color codes are as in Figure 5.

Velocities in the boundary current were highly variable and linear positive trends in velocity were comparatively small ($STD > 5\text{--}6$ cm/s, Figures 7c and 10c; trends of $+1\text{--}2$ cm/s/decade, Figures 7g and 10g). The boundary current exhibited an overall warming and salinification in the upper 100 m, reaching $+1^\circ\text{C}\text{--}2^\circ\text{C}$ /decade and $+0.2$ g/kg/decade. Below 100 m, temperature increased by about $+0.5^\circ\text{C}$ /decade and density decreased by -0.05 kg/m³/decade, likely due to a mild salinity decrease (Figures 7d, 7e, 10d, and 10e). The AW layer thickened over the lower slope in the boundary current, by $+200$ m/decade at the upstream AWBC1 (Figure 7h) and about $+50$ m/decade at A-TWAIN (Figure 10h).

4.3. Offshore AW Circulation

The western and eastern parts (OS1 and OS2, Figure 5) of the offshore circulation (purple arrows in Figure 14) carried relatively cold and fresh waters in 2008–2010 ($\Theta < 1.8^\circ\text{C}$, $S_A < 35.05$ g/kg at 265 m; Figures 9a, 10a and 10b). From 2011-onwards, the flow across OS1 and OS2 at 265 m mostly comprised AW (with $\Theta > 1.5^\circ\text{C}$, $S_A > 35.05$ g/kg), in spite of occurrences of colder, fresher waters (e.g., winter 2013/2014, years 2015, 2017) (Figures 9a, 9b, 10a, and 10b). The offshore circulation showed up as large positive (eastward) cross-section velocity trends in transects 2 and 3 ($+2$ to $+3$ cm/s/decade, Figures 9g and 10g).

The circulation across OS1 at 265m evolved from a weak ($V_x < 2$ cm/s) flow in 2008–2015, adjusting into a stronger and more organized flow from 2015-onwards (Figure 9c). The eastern part of the offshore circulation (OS2) at 265 m strengthened earlier in winter 2009/2010 ($V_x > 2$ cm/s, Figure 10c). As a result, AW volume transport across OS1 remained small until 2014 (< 0.25 Sv) and increased abruptly in 2015 to reach $0.5\text{--}0.75$ Sv in 2016–2020, while the AW transport at OS2 was moderate ($0.25\text{--}0.75$ Sv) in 2009–2014 and exceeded 0.5 Sv from 2015-onwards (Figures 11b).

The western part of the offshore circulation (OS1) was regularly fed by the YB reaching the Yermak Plateau tip, either flowing along the western edge of Yermak Plateau (plain yellow arrow in Figure 14), or through shortcuts across the Plateau (dashed yellow arrows in Figure 14), and joining the northeastward flow in the Sofia Deep (green arrows in Figure 14; supporting information S2). Furthermore, the cyclonic recirculation centered around 24°E , 83.8°N (gray arrow in Figure 14) recurrently advected colder and fresher waters from the deep WNB interior ($> 3,900$ m isobaths) toward OS1 (Figures 4c–4h). Interestingly, waters carried across OS2 were on average warmer and saltier than at OS1 ($\Theta \sim +0.4^\circ\text{C}$, $S_A \sim +0.02$ g/kg), indicating an additional contribution from the boundary current through enhanced basin-ward mesoscale activity injecting AW offshore.

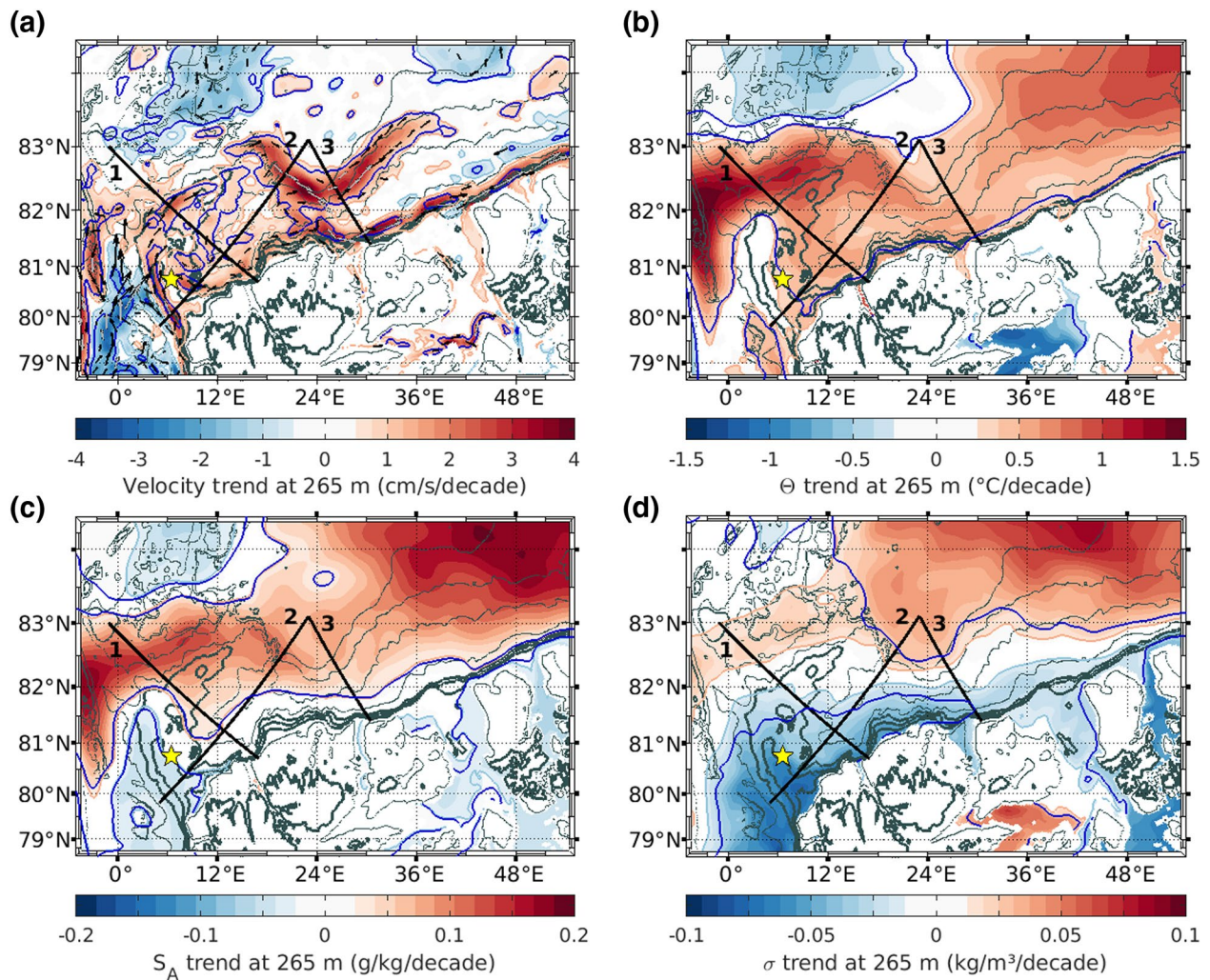


Figure 12. (a) Linear velocity trends (cm/s/decade) at 265 m, computed over a 12-year period (2008–2020). Velocity trend vectors are plotted in black arrows (gray arrows) for intensity trends larger than ± 1 cm/s/decade (± 2.5 cm/s/decade). (b) Linear trends of Conservative Temperature (Θ , $^{\circ}\text{C}/\text{decade}$) at 265 m. (c) Same for Absolute Salinity trends (S_A , g/kg/decade) and (d) potential density trends (σ , $\text{kg}/\text{m}^3/\text{decade}$). For (a–d), values under the 99.9% significance level are whitened. Blue contours delineate points where the 12-years trend is larger than the STD. The yellow star is the location of the mooring as in Figure 1. Isobaths contours are as in Figure 4. Thick black lines numbered 1 to 3 are the transects presented in Figures 7, 9, and 10.

5. Changes in AW Properties and Pathways in the WNB over 2008–2020

Velocity trends at 265 m highlighted the major circulation changes that is, the intensification of the YB at 82°N (with a local significant maximum of $+3$ cm/s/decade) and the development of the “V-shaped” offshore circulation (with a salient trend of $+4$ cm/s/decade) (Figure 12a). Other interesting features were the velocity decrease in the recirculation branches around the Molloy Deep (79°N) (-2 cm/s/decade) and intensification of recirculations north of 82°N (up to $+2$ cm/s/decade) (Figure 12a). The boundary current exhibited large positive velocity trends in the vicinity of trough openings: this could indicate enhanced instabilities and mesoscale activity, such as the frequent meandering described in Section 4.2.

Positive trends in temperature and salinity at 265 m (core of the AW layer, Figures 12b and 12c) were consistent with these strengthening AW pathways (Figure 12a). Large positive trends to the north and northwest of Yermak Plateau (up to $+1.5^{\circ}\text{C}/\text{decade}$, $+0.15$ g/kg/decade, $+0.03$ $\text{kg}/\text{m}^3/\text{decade}$; Figures 12b–12d) corresponded to the intensification of the YB and northward shift of AW recirculation branches (Figure 12a). Another large increase in temperature, salinity and density at 265 m was located northeast of 83°N , 30°E (Figures 12b–12d) downstream of the intensifying “V-shaped” offshore circulation, bringing more warm and salty AW from the boundary current toward the basin interior (Figure 12a).

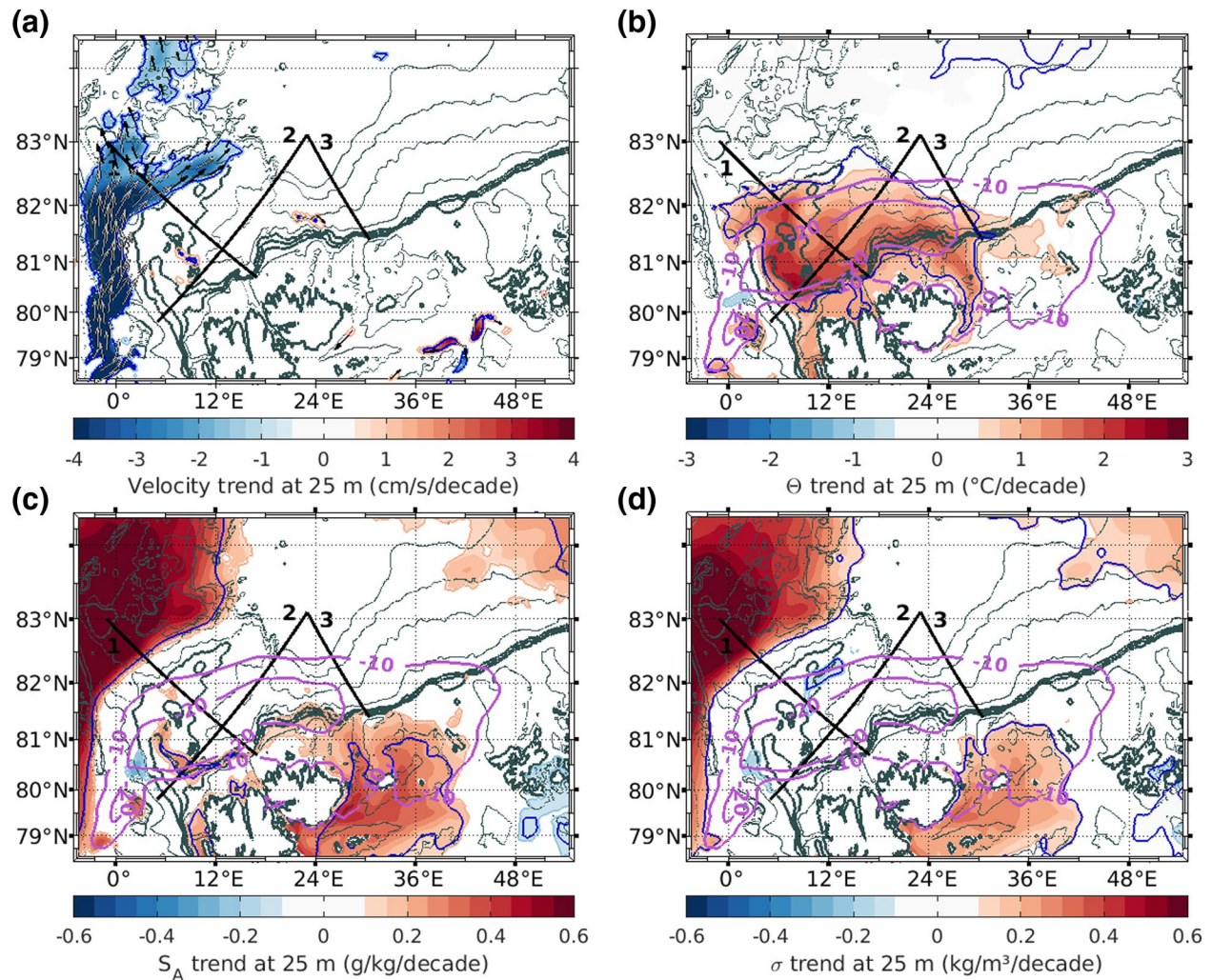


Figure 13. (a) Linear velocity trends (cm/s/decade) at 25 m, computed over a 12-year period (2008–2020). Velocity trend vectors are plotted in black arrows (gray arrows) for intensity trends larger than ± 1 cm/s/decade (± 2.5 cm/s/decade). (b) Linear trends of Conservative Temperature (Θ , $^{\circ}\text{C}/\text{decade}$) at 25 m. (c) Same for Absolute Salinity trends (S_A , g/kg/decade) and (d) potential density trends (σ , $\text{kg}/\text{m}^3/\text{decade}$). For (a–d), values under the 99.9% significance level are whitened. The pink contours on (b–d) are the -10% and -20% trends in sea-ice cover (%/decade). Blue contours delineate points where the 12-year trend is larger than the STD. Isobaths contours are as in Figure 4. Thick black lines numbered 1 to 3 are the transects presented in Figures 7, 9, and 10.

The warming AW inflow ($+0.5^{\circ}\text{C}/\text{decade}$, Figure 12b) exhibited notable freshening in 2018–2020 (Figures 9a, 9b, and 12c). This recent salinity decrease was consistent with the 2017–2020 mooring data in the YPB (Figures 2b and 2d) and likely caused by the propagation of extreme fresh anomalies observed in 2012–2018 in the upstream North Atlantic and Norwegian Sea (Holliday et al., 2020; Mork et al., 2019). As a result, the density decreased along the slope south of 82°N at 265 m ($-0.05 \text{ kg}/\text{m}^3/\text{decade}$, Figure 12d) in the 100–900 m layer (Figures 7f, 9f, and 10f). As discussed in section 4, the significant warming spread over the upper 1,000 m of the WNB and was maximum in the upper 200 m ($+2^{\circ}\text{C}/\text{decade}$) (Figures 7d, 9d, and 10d). This near-surface warming was associated with a maximum salinity increase (exceeding $+0.2 \text{ g}/\text{kg}/\text{decade}$ at 100 m) (Figures 7e, 9e, and 10e) and the shoaling of the AW layer.

Near the surface, negative velocity trends west of 0°E (-1 to $-4 \text{ cm}/\text{s}/\text{decade}$) possibly indicated a reduction or shift of the Transpolar Drift (TPD) and the increasing influence of the YB near the surface on the north-western flank of Yermak Plateau (Figure 13a).

The warming trend at 25 m, reaching $2.5^{\circ}\text{C}/\text{decade}$ over the YPB, did not extend further than 83°N and coincided with a sea-ice cover decline larger than $-10\%/decade$ (reaching up to $-30\%/decade$ over YPB; Figure 13b). A striking signal in salinity and density at 25 m was the dramatic positive trends within the

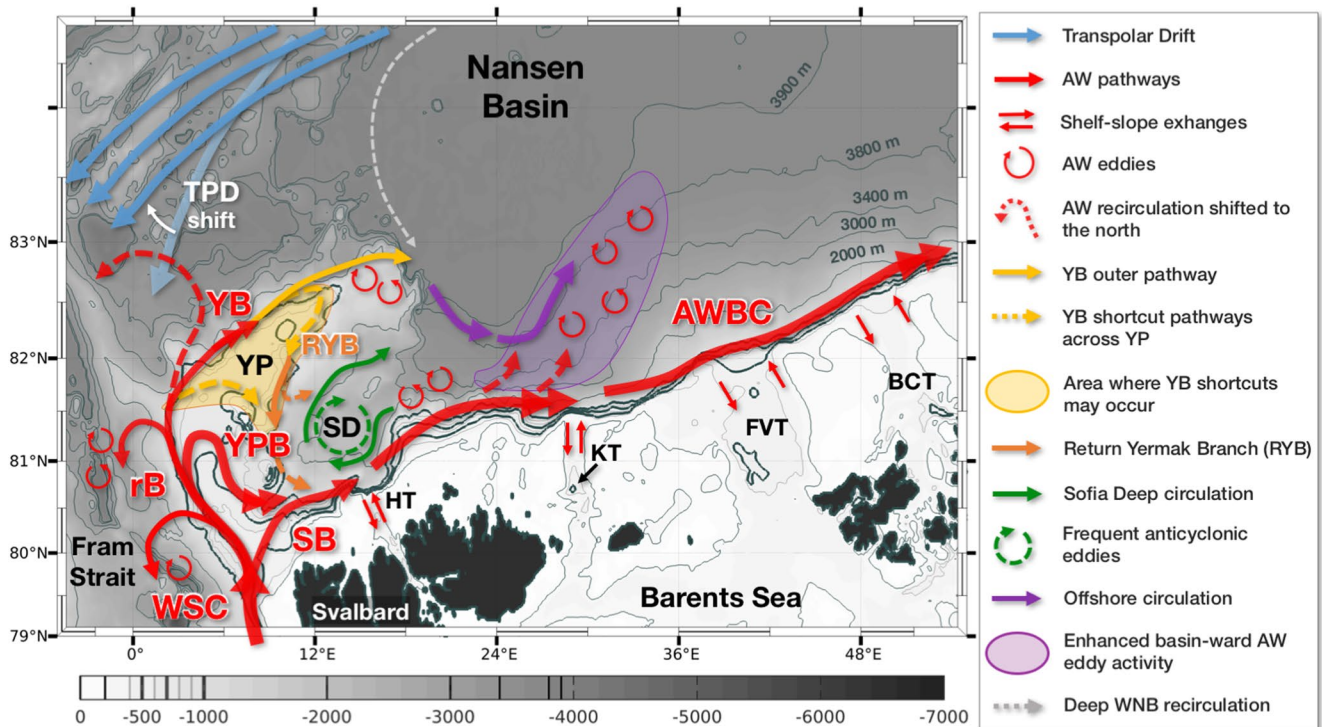


Figure 14. Schematic circulation and water pathways over the Yermak Plateau and in the WNB in the recent 2011–2020 period, as suggested by PSY4. Blue arrows represent the near-surface Transpolar Drift (TPD). Red arrows are the Atlantic Water (AW) circulation documented in the literature; orange, green and purple arrows are the newly suggested AW pathways. AWBC, AW Boundary Current; HT, KT, FVT, and BCT, Hinlopen, Kvitøya, Franz-Victoria, and British Channel Troughs; rB, recirculation Branches; RYB, Return Yermak Branch; SB, Svalbard Branch; SD, Sofia Deep; WSC, West Spitsbergen Current; YB, Yermak Branch; YP, Yermak Plateau; YPB, Yermak Pass Branch.

Transpolar Drift pathway (blue in Figure 13a), centered around 83°N, 0°E ($>+0.6$ g/kg/decade, $+0.5$ kg/m³/decade; Figures 7e, 7f, 13c, and 13d). Along transect 1, salinity at 25 m showed the northwestward AW progression, and the reducing ice cover allowed the atmosphere to maintain close-to-freezing temperatures (not shown).

There were no significant trends in salinity and density at 25 m in the WNB interior; however, the continental shelf exhibited positive trends exceeding local STD values ($+0.2$ g/kg/decade, $+0.15$ kg/m³/decade; Figures 13c and 13d). This could be due to a change in the upstream Barents Sea conditions, out of the scope of this study.

6. Summary and Discussion

We used 12 years of PSY4 fields to examine the evolution of the circulation, volume transport and properties of AW in their major entry region, the WNB. Previous examination of the model performance in the WNB underlined the good skill of PSY4 in representing realistic AW inflow and properties (Athanasé et al., 2020), despite some inherent limitations. Indeed, the model is not fully eddy-resolving in the area (i.e., grid size of 4 km, and Rossby deformation radius of ~ 10 km; Crews et al., 2018) and does not simulate tides which are important above and on the slopes of the Yermak Plateau (e.g., Fer et al., 2020; Koenig et al., 2017a; Padman et al., 1992). Further comparisons with a 32 months-long (2017–2020) time-series of temperature and salinity at 350 m in the Yermak Pass (Labaste et al., 2020) and with a CNES/CLS multi-mission altimetry product prototype for the Arctic Ocean (2016–2018) confirmed the good performance of PSY4 in recent years (Figure 2). The skill of the model in reproducing the properties and velocity in the AW boundary current was further demonstrated by comparing modeled and observed AW volume transport at 30°E in 2012–2013 (correlation of $r = 0.79$ with 10-days smoothed A-TWAIN observations, significant at the 99% confidence level) (Figure 3). PSY4 was thus trusted to examine AW circulation and volume transport in the WNB.

Circulation patterns at 265 m have changed in the WNB over 2008–2020 (compare Figure 14 and Figure 1; trends in Figures 12 and 13). Major changes include the strengthening of the YB (yellow arrows in Figure 14) feeding the RYB along the eastern flank of the Plateau (orange arrows). Downstream of Yermak Plateau, a circulation developed offshore following a V-shape above isobaths 3,800–3,900 m (purple arrows). The western part of the offshore flow was fed with waters from the Yermak Plateau tip starting in 2015. As early as 2009, enhanced basin-ward mesoscale activity contributed to the northeastward part of the offshore current, bringing warm and salty AW (purple area in Figure 14). Indeed, the AWBC strengthened east of 18°E, with more frequent meandering (schematized with double red arrows in Figure 14). A recurrent anticyclonic circulation developed in Sofia the Deep, either via long-lived eddies or anticyclonic meanders (green arrows), which also occasionally fed the western part of the offshore flow. West of Yermak Plateau, the Transpolar Drift likely shifted westward (blue arrows) while AW recirculations progressed further north (dashed red arrow).

These circulation changes have yet to be considered with caution. Indeed, it is possible that the offshore intensification from 2011-onwards could result from a spin-up period larger than the 15 months estimated here (see Appendix), due to particularly small velocities in the WNB interior (about 2–3 cm/s). Nonetheless, the changes were consistent with the few available observational studies. The development of the offshore circulation was concordant with the existence of a local minimum in SSH fields north of the 3,800 m isobath (see Section 2.2.), inducing horizontal SSH gradients along the 3,800–3,900 m isobaths and thus surface geostrophic velocities. Furthermore, several studies documented AW mesoscale structures along the track of the eastern, basin-ward part of the offshore flow (Athanasé et al., 2019; Pérez-Hernández et al., 2017; Våge et al., 2016). Observations over the continental slope also supported the evolution of the boundary current: indeed, V. V. Ivanov et al. (2009) reported a highly persistent direction of the flow in the AWBC near 30°E in 2004, while at the same location the boundary current was observed to be baroclinically unstable, meandering across the slope and shedding eddies in 2012–2013 (Pérez-Hernández et al., 2017, 2019; Våge et al., 2016). Recent in situ data from Kolås et al. (2020) in summer and fall 2018 in the Sofia Deep documented a westward countercurrent just to the north of the boundary current in the Sofia Deep and detaching from the slope at 18°E, in agreement with the modeled anticyclonic circulation in Sofia Deep. Finally, a meander of AW turning back toward Fram Strait was observed at 82.8°N, 3°W in December 2017 (Athanasé et al., 2019), supporting the northward shift of recirculation branches.

The intensification of the circulation coincided with an overall warming and salinification in the upper 1,000 m of the WNB interior, consistent with the progression of AW in the region (Figures 7, 9, 10, and 12b). Interestingly, the warming AW inflow exhibited negative salinity trends (Figure 12c), resulting from a notable freshening in 2018–2020 (Figures 7a, 7b, 9a, 9b, 10a and 10b). The recent 2017–2020 mooring data in the YPB further documented this salinity decrease (Figures 2b and 2d). The freshening of the AW inflow was in agreement with the extreme fresh anomalies observed in the upstream North Atlantic in 2012–2016 and in the Norwegian Sea in 2017–2018, caused by wind-driven changes in the ocean circulation which advected fresher waters of Arctic origin into the subpolar North Atlantic (Holliday et al., 2020; Mork et al., 2019). This underlines the crucial role of upstream atmospheric and oceanic conditions in determining the properties of AW entering the Arctic.

PSY4 yielded insights on AW pathways and volume transports in the rapidly transitioning WNB. This regional description of the changing circulation provides a background for the interpretation of upcoming mooring and synoptic cruise data, which might revise the present conclusions.

Appendix: Initial Conditions In The PSY4 System

The PSY4 system was initialized with temperature and salinity from EN4.2.1 fields in October 2006 (Good et al., 2013). The October 2006 salinity field exhibited an unexpected pattern with a local minimum (S_A (265 m) < 34.9 g/kg) radiating from the Franz-Josef shelf toward the pole along the 50°E longitude (Figure A1), likely created by undesirable interpolations or extrapolations of remote observations in this data-sparse area.

Time-series of vertical profiles in the spurious initial salinity minimum at 55°E (Figures A1d and A1e) illustrate the evolution of temperature and salinity from these initial conditions. In the AW layer (265 m), AW salinity near 50°E decreased sharply from its anomalously fresh values until stabilizing around 35 g/kg in early 2008. Hence, the spin-up time in the WNB was considered to be 15 months and time-series were only considered from April 2008 onwards.

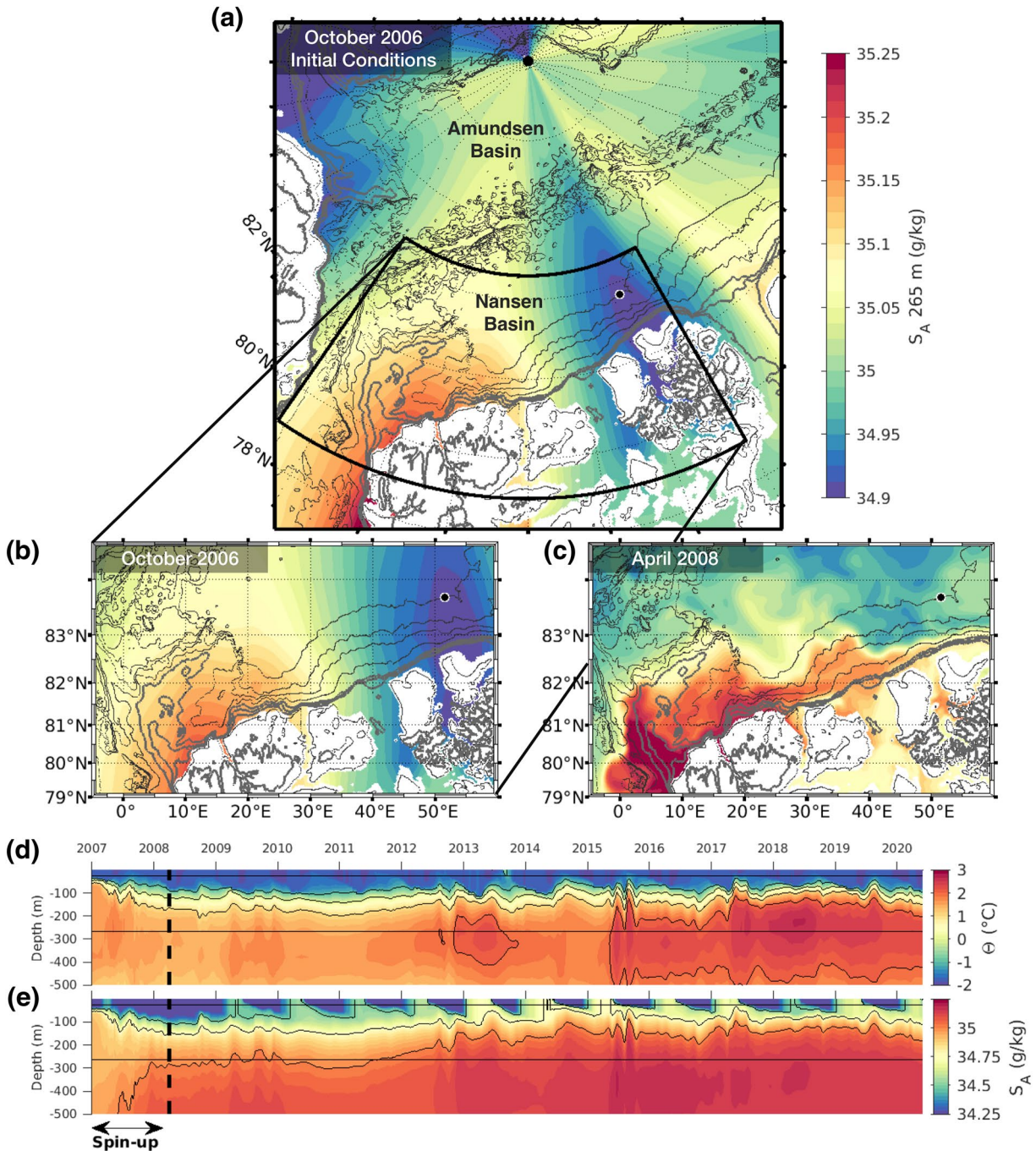


Figure A1. (a) Initial conditions of the PSY4 system in October 2006 over the Western Eurasian Basin, in Absolute Salinity (S_A , g/kg) at 265 m. Gray contours is the IBCAO bathymetry. (b) Same as (a), focused on the Western Nansen Basin (WNB) area (black box on [a]). (c) Absolute Salinity (g/kg) at 265 m, in April 2008. (d) Time-series (upper 500 m) of Conservative Temperature (θ , °C) and (e) Absolute Salinity (g/kg) at the location of the initial local salinity minimum (black point on [a]–[c]). Depths 25 and 265 m are reported as horizontal lines. The spin-up period (January 2007–April 2008) for the WNB area is delineated by the thick dashed line.

Indeed, the WNB region considered here constitutes in a trapeze-shaped area of 600 km width (north-south), and minimum (northern edge) and maximum (southern edge) length of 600 and 1,200 km. In this region, the assimilation of parameters other than sea-ice are primarily confined to the ice-free Fram Strait. Times of advection from Fram Strait to the ice-covered basin interior were estimated to be roughly on the order of 10–15 months.

The computations shown in the manuscript were also performed on a shorter time-series (April 2009 to May 2019) and the results were not significantly different.

Data Availability Statement

The model outputs are available at Copernicus Marine Environment Monitoring Service (CMEMS; <http://marine.copernicus.eu/>).

Acknowledgments

We gratefully acknowledge all the people that contributed to gather the observations used for model validation in this study. Marylou Athanase was supported through the Pan-Arctic Options Belmont Forum project (ANR-14-AORS-003-01), Cecilia Bertosio through IAOS grant A18JROI002 at Sorbonne University, and M. Dolores Pérez-Hernández through the “Programa Postdoctoral de la Universidad de Las Palmas de Gran Canaria.” We are deeply grateful to editor Laurie Padman and two anonymous reviewers, whose detailed comments and suggestions helped improve the manuscript.

References

- Athanase, M., Provost, C., Pérez-Hernández, M. D., Sennéchaël, N., Bertosio, C., Artana, C., et al. (2020). Atlantic water modification north of Svalbard in the Mercator physical system from 2007 to 2020. *Journal of Geophysical Research: Oceans*, *125*(10), e2020JC016463. <https://doi.org/10.1029/2020JC016463>
- Athanase, M., Sennéchaël, N., Garric, G., Koenig, Z., Boles, E., & Provost, C. (2019). New hydrographic measurements of the upper arctic Western Eurasian Basin in 2017 reveal fresher mixed layer and shallower warm layer than 2005–2012 climatology. *Journal of Geophysical Research: Oceans*, *124*(2), 1091–1114. <https://doi.org/10.1029/2018JC014701>
- Bertosio, C., Provost, C., Sennéchaël, N., Artana, C., Athanase, M., Boles, E., et al. (2020). The Western Eurasian Basin halocline in 2017: Insights from autonomous NO measurements and the Mercator physical system. *Journal of Geophysical Research: Oceans*, *125*(7), e2020JC016204. <https://doi.org/10.1029/2020JC016204>
- Beszczynska-Möller, A., Fahrbach, E., Schauer, U., & Hansen, E. (2012). Variability in Atlantic water temperature and transport at the entrance to the Arctic Ocean, 1997–2010. *ICES Journal of Marine Science*, *69*(5), 852–863. <https://doi.org/10.1093/icesjms/fss056>
- Boyd, T. J., & D'Asaro, E. A. (1994). Cooling of the West Spitsbergen Current: Wintertime observations West of Svalbard. *Journal of Geophysical Research: Oceans*, *99*(C11), 22597–22618. <https://doi.org/10.1029/94JC01824>
- Bretherton, F. P., Davis, R. E., & Fandry, C. B. (1976). A technique for objective analysis and design of oceanographic experiments applied to MODE-73. *Deep-Sea Research and Oceanographic Abstracts*, *23*(7), 559–582. [https://doi.org/10.1016/0011-7471\(76\)90001-2](https://doi.org/10.1016/0011-7471(76)90001-2)
- Cokelet, E. D., Tervalon, N., & Bellingham, J. G. (2008). Hydrography of the West Spitsbergen Current, Svalbard Branch: Autumn 2001. *Journal of Geophysical Research*, *113*, C01006. <https://doi.org/10.1029/2007JC004150>
- Crews, L., Sundfjord, A., Albretsen, J., & Hattermann, T. (2018). Mesoscale eddy activity and transport in the Atlantic Water inflow region north of Svalbard. *Journal of Geophysical Research: Oceans*, *123*, 201–215. <https://doi.org/10.1002/2017JC013198>
- Crews, L., Sundfjord, A., & Hattermann, T. (2019). How the Yermak Pass Branch regulates Atlantic water inflow to the Arctic Ocean. *Journal of Geophysical Research: Oceans*, *124*(1), 267–280. <https://doi.org/10.1029/2018JC014476>
- Ducet, N., Le Traon, P. Y., & Reverdin, G. (2000). Global high-resolution mapping of ocean circulation from TOPEX/Poseidon and ERS-1 and -2. *Journal of Geophysical Research*, *105*(C8), 19477–19498. <https://doi.org/10.1029/2000JC900063>
- Fer, I., Koenig, Z., Kozlov, I. E., Ostrowski, M., Rippeth, T. P., Padman, L., et al. (2020). Tidally forced lee waves drive turbulent mixing along the Arctic Ocean margins. *Geophysical Research Letters*, *47*, e2020GL088083. <https://doi.org/10.1029/2020GL088083>
- Good, S. A., Martin, M. J., & Rayner, N. A. (2013). EN4: Quality controlled ocean temperature and salinity profiles and monthly objective analyses with uncertainty estimates. *Journal of Geophysical Research: Oceans*, *118*, 6704–6716. <https://doi.org/10.1002/2013JC009067>
- Hattermann, T., Isachsen, P. E., von Appen, W. J., Albretsen, J., & Sundfjord, A. (2016). Eddy-driven recirculation of Atlantic water in Fram Strait. *Geophysical Research Letters*, *43*(7), 3406–3414. <https://doi.org/10.1002/2016GL068323>
- Holliday, N. P., Bersch, M., Berx, B., Chafik, L., Cunningham, S., Florindo-López, C., et al. (2020). Ocean circulation causes the largest freshening event for 120 years in eastern subpolar North Atlantic. *Nature Communications*, *11*(1), 1–15. <https://doi.org/10.1038/s41467-020-14474-y>
- Hu, X., Myers, P. G., & Lu, Y. (2019). Pacific water pathway in the Arctic Ocean and Beaufort Gyre in two simulations with different horizontal resolutions. *Journal of Geophysical Research: Oceans*, *124*(8), 6414–6432. <https://doi.org/10.1029/2019JC015111>
- Ivanov, V. V., Polyakov, I. V., Dmitrenko, I. A., Hansen, E., Repina, I. A., Kirillov, S. A., et al. (2009). Seasonal variability in Atlantic water off Spitsbergen. *Deep Sea Research Part I: Oceanographic Research Papers*, *56*(1), 1–14. <https://doi.org/10.1016/j.dsr.2008.07.013>
- Ivanov, V., Smirnov, A., Alexeev, V., Koldunov, N. V., Repina, I., & Semenov, V. (2018). Contribution of convection-induced heat flux to winter ice decay in the Western Nansen Basin. *Journal of Geophysical Research: Oceans*, *123*(9), 6581–6597. <https://doi.org/10.1029/2018JC013995>
- Jakobsson, M., Mayer, L., Coakley, B., Dowdeswell, J. A., Forbes, S., Fridman, B., et al. (2012). The international bathymetric chart of the Arctic Ocean (IBCAO) version 3.0. *Geophysical Research Letters*, *39*, L12609. <https://doi.org/10.1029/2012GL052219>
- Koenig, Z., Meyer, A., Provost, C., Sennéchaël, N., Sundfjord, A., Beguery, L., et al. (2018). Cooling and freshening of the West Spitsbergen Current by shelf-origin cold core lenses. *Journal of Geophysical Research: Oceans*, *123*(11), 8299–8312. <https://doi.org/10.1029/2018JC014463>
- Koenig, Z., Provost, C., Sennéchaël, N., Garric, G., & Gascard, J.-C. (2017a). The Yermak Pass Branch: A major pathway for the Atlantic water North of Svalbard?. *Journal of Geophysical Research: Oceans*, *122*(12), 9332–9349. <https://doi.org/10.1002/2017JC013271>
- Koenig, Z., Provost, C., Villacieros-Robineau, N., Sennéchaël, N., Meyer, A., Lellouche, J.-M., & (2017b). Atlantic waters inflow north of Svalbard: Insights from IAOS observations and Mercator Ocean global operational system during N-ICE2015. *Journal of Geophysical Research: Oceans*, *122*, 1254–1273. <https://doi.org/10.1002/2016JC012424>
- Kolås, E. H., Koenig, Z., Fer, I., Nilsen, F., & Marnela, M. (2020). Structure and transport of Atlantic Water north of Svalbard from observations in summer and fall 2018. *Journal of Geophysical Research: Oceans*, *125*(9), e2020JC016174. <https://doi.org/10.1029/2020JC016174>

- Labaste, M., Gascard, J.-C., Provost, C., Sennéchaël, N., & Athanase, M. (2020). Yermak Plateau mooring: SBE37 CTD at 350 m, in 2017–2020. SEANO. <https://doi.org/10.17882/76330>
- Lellouche, J. M., Greiner, E., Le Galloudec, O., Garric, G., Regnier, C., Drevillon, M., et al. (2018). Recent updates to the Copernicus Marine Service global ocean monitoring and forecasting real-time 1/12° high-resolution system. *Ocean Science*, 14(5), 1093–1126. <https://doi.org/10.5194/os-14-1093-2018>
- Manley, T. O. (1995). Branching of Atlantic water within the Greenland-Spitsbergen passage: An estimate of recirculation. *Journal of Geophysical Research*, 100(C10), 20627–20634. <https://doi.org/10.1029/95JC01251>
- Manley, T. O., Bourke, R. H., & Hunkins, K. L. (1992). Near-surface circulation over the Yermak Plateau in northern Fram Strait. *Journal of Marine Systems*, 3(1–2), 107–125. [https://doi.org/10.1016/0924-7963\(92\)90033-5](https://doi.org/10.1016/0924-7963(92)90033-5)
- Menze, S., Ingvaldsen, R. B., Haugan, P., Fer, I., Sundfjord, A., Beszczynska-Moeller, A., & (2019). Atlantic water pathways along the north-western Svalbard shelf mapped using vessel-mounted current profilers. *Journal of Geophysical Research: Oceans*, 124(3), 1699–1716. <https://doi.org/10.1029/2018JC014299>
- Meyer, A., Sundfjord, A., Fer, I., Provost, C., Villaceros Robineau, N., Koenig, Z., et al. (2017). Winter to summer oceanographic observations in the Arctic Ocean north of Svalbard. *Journal of Geophysical Research: Oceans*, 122(8), 6218–6237. <https://doi.org/10.1002/2016JC012391>
- Mork, K. A., Skagseth, Ø., & Soiland, H. (2019). Recent warming and freshening of the Norwegian Sea observed by Argo data. *Journal of Climate*, 32(12), 3695–3705. <https://doi.org/10.1175/JCLI-D-18-0591.1>
- Muench, R. D., McPhee, M. G., Paulson, C. A., & Morison, J. H. (1992). Winter oceanographic conditions in the Fram Strait-Yermak Plateau region. *Journal of Geophysical Research*, 97(C3), 3469–3483. <https://doi.org/10.1029/91JC03107>
- Onarheim, I. H., Smedsrud, L. H., Ingvaldsen, R. B., & Nilsen, F. (2014). Loss of sea ice during winter north of Svalbard. *Tellus A: Dynamic Meteorology and Oceanography*, 66(1), 23933. <https://doi.org/10.3402/tellusa.v66.23933>
- Padman, L., Plueddemann, A., Muench, R., & Pinkel, R. (1992). Diurnal tides near the Yermak Plateau. *Journal of Geophysical Research*, 97, 12639–12652. <https://doi.org/10.1029/92JC01097>
- Pérez-Hernández, M. D., Pickart, R. S., Pavlov, V., Våge, K., Ingvaldsen, R., Sundfjord, A., et al. (2017). The Atlantic Water boundary current north of Svalbard in late summer. *Journal of Geophysical Research: Oceans*, 122(3), 2269–2290. <https://doi.org/10.1029/2018JC014299>
- Pérez-Hernández, M. D., Pickart, R. S., Torres, D. J., Bahr, F., Sundfjord, A., Ingvaldsen, R., et al. (2019). Structure, transport, and seasonality of the Atlantic Water boundary current north of Svalbard: Results from a yearlong mooring Array. *Journal of Geophysical Research: Oceans*, 124(3), 1679–1698. <https://doi.org/10.1029/2018JC014759>
- Poisson, J., Quartly, G. D., Kurekin, A. A., Thibaut, P., Hoang, D., & Nencioli, F. (2018). Development of an ENVISAT Altimetry processor providing Sea Level continuity between Open Ocean and Arctic leads. *IEEE Transactions on Geoscience and Remote Sensing*, 56(9), 5299–5319. <https://doi.org/10.1109/TGRS.2018.2813061>
- Polyakov, I. V., Pnyushkov, A. V., Alkire, M. B., Ashik, I. M., Baumann, T. M., Carmack, E. C., et al. (2017). Greater role for Atlantic inflows on sea-ice loss in the Eurasian Basin of the Arctic Ocean. *Science*, 356(6335), 285–291. <https://doi.org/10.1126/science.aai8204>
- Polyakov, I. V., Rippeth, T. P., Fer, I., Baumann, T. M., Carmack, E. C., Ivanov, V. V., et al. (2020). Intensification of near-surface currents and shear in the Eastern Arctic Ocean. *Geophysical Research Letters*, 47(16), e2020GL089469. <https://doi.org/10.1029/2020GL089469>
- Renner, A. H. H., Sundfjord, A., Janout, M. A., Ingvaldsen, R., Beszczynska-Möller, A., Pickart, R., & (2018). Variability and redistribution of heat in the Atlantic Water boundary current north of Svalbard. *Journal of Geophysical Research: Oceans*, 123, 6373–6391. <https://doi.org/10.1029/2018JC013814>
- Rudels, B., Korhonen, M., Schauer, U., Pisarev, S., Rabe, B., & Wisotzki, A. (2015). Circulation and transformation of Atlantic water in the Eurasian Basin and the contribution of the Fram Strait inflow branch to the Arctic Ocean heat budget. *Progress in Oceanography*, 132, 128–152. <https://doi.org/10.1016/j.pocean.2014.04.003>
- Schauer, U., Muench, R. D., Rudels, B., & Timokhov, L. (1997). Impact of eastern Arctic shelf waters on the Nansen Basin intermediate layers. *Journal of Geophysical Research*, 102(C2), 3371–3382. <https://doi.org/10.1029/96JC03366>
- Sirevaag, A., de La Rosa, S., Fer, I., Nicolaus, M., Tjernström, M., & McPhee, M. G. (2011). Mixing, heat fluxes and heat content evolution of the Arctic Ocean mixed layer. *Ocean Science*, 7(3), 335–349. <https://doi.org/10.5194/os-7-335-2011>
- Timmermans, M.-L., & Marshall, J. (2020). Understanding Arctic Ocean circulation: A review of ocean dynamics in a changing climate. *Journal of Geophysical Research: Oceans*, 125, e2018JC014378. <https://doi.org/10.1029/2018JC014378>
- Våge, K., Pickart, R. S., Pavlov, V., Lin, P., Torres, D. J., Ingvaldsen, R., et al. (2016). The Atlantic Water boundary current in the Nansen Basin: Transport and mechanisms of lateral exchange. *Journal of Geophysical Research: Oceans*, 121, 6946–6960. <https://doi.org/10.1002/2016JC011715>
- Valladares, J., Fennel, W., & Morozov, E. (2011). Replacement of EOS-80 with the International Thermodynamic Equation of Seawater–2010 (TEOS-10). *Deep-Sea Res. Part. I*, 58, 978. <https://doi.org/10.1016/j.dsr.2011.07.005>